

Article

Experimental Assessment of the Reflection of Solar Radiation from Façades of Tall Buildings to the Pedestrian Level

Alberto Speroni ¹, Andrea Giovanni Mainini ^{1,*} , Andrea Zani ^{1,2}, Riccardo Paolini ³ , Tommaso Pagnacco ^{1,4} and Tiziana Poli ¹ 

- ¹ Architecture, Built Environment and Construction Engineering Department, Politecnico di Milano, Via Ponzio 31, 20133 Milano, Italy; alberto.speroni@polimi.it (A.S.); a.zani@permasteelisagroup.com (A.Z.); tpagnacco@bollinger-grohmann.it (T.P.); tiziana.poli@polimi.it (T.P.)
- ² Permasteelisa North America, 1179 Centre Pointe Circle, Mendota Heights, MN 55120, USA
- ³ School of Built Environment, Faculty of Arts, Design & Architecture, University of New South Wales, Sydney, NSW 2052, Australia; r.paolini@unsw.edu.au
- ⁴ Bollinger + Grohmann Ingegneria, Via Garofalo 31, 20133 Milano, Italy
- * Correspondence: andreagiovanni.mainini@polimi.it; Tel.: +39-022-399-6015

Abstract: Urban climates are highly influenced by the ability of built surfaces to reflect solar radiation, and the use of high-albedo materials has been widely investigated as an effective option to mitigate urban overheating. While diffusely solar reflective walls have attracted concerns in the architectural and thermal comfort community, the potential of concave and polished surfaces, such as glass and metal panels, to cause extreme glare and localized thermal stress has been underinvestigated. Furthermore, there is the need for a systematic comparison of the solar concentration at the pedestrian level in front of tall buildings. Herein, we show the findings of an experimental campaign measuring the magnitude of the sunlight reflected by scale models reproducing archetypical tall buildings. Three 1:100 scaled prototypes with different shapes (classic vertical façade, 10% tilted façade, curved concave façade) and different finishing materials (representative of extremes in reflectance properties of building materials) were assessed. A specular surface was assumed as representative of a glazed façade under high-incidence solar angles, while selected light-diffusing materials were considered sufficient proxies for plaster finishing. With a diffusely reflective façade, the incident radiation at the pedestrian level in front of the building did not increase by more than 30% for any geometry. However, with a specular reflective (i.e., mirror-like) flat façade, the incident radiation at the pedestrian level increased by more than 100% and even by more than 300% with curved solar-concentrating geometries. In addition, a tool for the preliminary evaluation of the solar reflectance risk potential of a generic complex building shape is developed and presented. Our findings demonstrate that the solar concentration risk due to mirror-like surfaces in the built environment should be a primary concern in design and urban microclimatology.

Keywords: reflective materials; mitigation; urban heat island; outdoor comfort; visual comfort; heat stress; optimization; skyscrapers



Citation: Speroni, A.; Mainini, A.G.; Zani, A.; Paolini, R.; Pagnacco, T.; Poli, T. Experimental Assessment of the Reflection of Solar Radiation from Façades of Tall Buildings to the Pedestrian Level. *Sustainability* **2022**, *14*, 5781. <https://doi.org/10.3390/su14105781>

Academic Editor: Baojie He

Received: 17 March 2022

Accepted: 26 April 2022

Published: 10 May 2022

Publisher's Note: MDPI stays neutral with regard to jurisdictional claims in published maps and institutional affiliations.



Copyright: © 2022 by the authors. Licensee MDPI, Basel, Switzerland. This article is an open access article distributed under the terms and conditions of the Creative Commons Attribution (CC BY) license (<https://creativecommons.org/licenses/by/4.0/>).

1. Introduction and State of the Art

The accelerating city climate change in combination with local and global climate change heightens the need for decarbonization of the built environment through energy efficiency and mitigation of urban overheating [1]. In particular, solar reflective roofs and walls have been largely investigated to reduce the solar absorption by the urban envelope and thus reduce the release of turbulent sensible heat that increases the ambient temperature [2,3]. Cool surfaces have high reflectance and emissivity and are capable of reducing both solar gains and surface temperatures, positively affecting the energy use of the building and helping to mitigate heat island effects at the mesoscale and local level [4–8]. Heat mitigation technologies can reduce the ambient temperature by 2–2.5 °C

when combined with building positive synergies, with the reduction of the solar gains being one of the main pathways to minimize urban overheating [9]. Cool walls in Los Angeles, for instance, may reduce the peak temperature by approximately 0.60 °C [2]. Furthermore, increasing the albedo of walls by 0.10 reduces the cooling energy needs of residential buildings in Mediterranean climates by 2.9 kWh/m² and reduces the indoor operative temperature of unconditioned buildings by 1.1 °C [10]. While the use of solar-reflective walls has been common in the Mediterranean and other vernacular architecture, there is an increasing concern among architects and urban designers about the potential increased solar reflection towards pedestrians [11,12]. While there are some limitations in current outdoor thermal comfort models, the need to limit the downward reflection of solar radiation towards the bottom of street canyons has received considerable attention in the literature [13–15]. This led to the identification and testing of retro-reflective surfaces as an option to minimize the shortwave radiation entrapment within the urban canopy layer [16]. Retro-reflective materials reflect the direct component of the solar radiation back towards the sun, thus upwards and not directed towards other urban surfaces. However, the proliferation in the use of specular reflective (i.e., mirror-like) materials in architecture has been underinvestigated with respect to their impact on outdoor visual and thermal comfort.

The research of eye-catching shapes for tall buildings, without considering its impact on the urban context [17,18], sometimes leads to increased incident solar radiation on other buildings and at street level due to unwanted reflections [19]. This phenomenon is due to the geometry being able to concentrate increasing solar radiation and the materials used in façade applications, especially high-reflectance glass or polish metal. Considering the transparent part of the building envelope, reflecting glazing systems with a reflectivity of more than 30–40% are chosen to reduce the cooling load of office and commercial buildings with large, exposed curtain walls. Reflectance properties of glazing are angular-dependent and influenced by the direction of the light source falling on their surface. The more the rays strike toward a direction parallel to the surface, the more the reflectance of the surface rapidly increases [20]. This is the case, for example, in temperate climates, particularly during the winter months, for surfaces facing south and during the early and late hours of the day, or in tropical climates for the same orientation and during the central hours of the day. High-reflectance surface treatment increases the possibility of external reflections for lower incidence angles as well.

Most unwanted reflections affect the vision and the visual comfort of pedestrians, users of concurrent buildings, car drivers, train conductors, and plane pilots [21]. The temporary visual disabilities resulting from these phenomena can also raise security issues by potentially causing an accident due to visual impairment, risking people's lives. Glare has also been reported as a critical issue in an urban environment, concerning angular reflective surfaces such as Photovoltaic panels [22] or concentrating solar collector plants with small and large highly reflective surfaces [23].

More disturbing effects have been reported when concentrated solar energy led to direct damage of properties, plants, and people caused by increased and focused solar radiation. The consequences of these effects can be temporary or repeated cyclically during the day/year, depending on the location, orientation, and urban context. Among the most significant cases are the "20 Fenchurch Street" building in London (Figure 1a, Table 1) and the "Vdara" building in Las Vegas (Table 1), which obliged the owners to either modify the façade or change the previously programmed use of the surrounding area in order to provide for costly subsequent mitigation and unplanned mitigation measures [24].

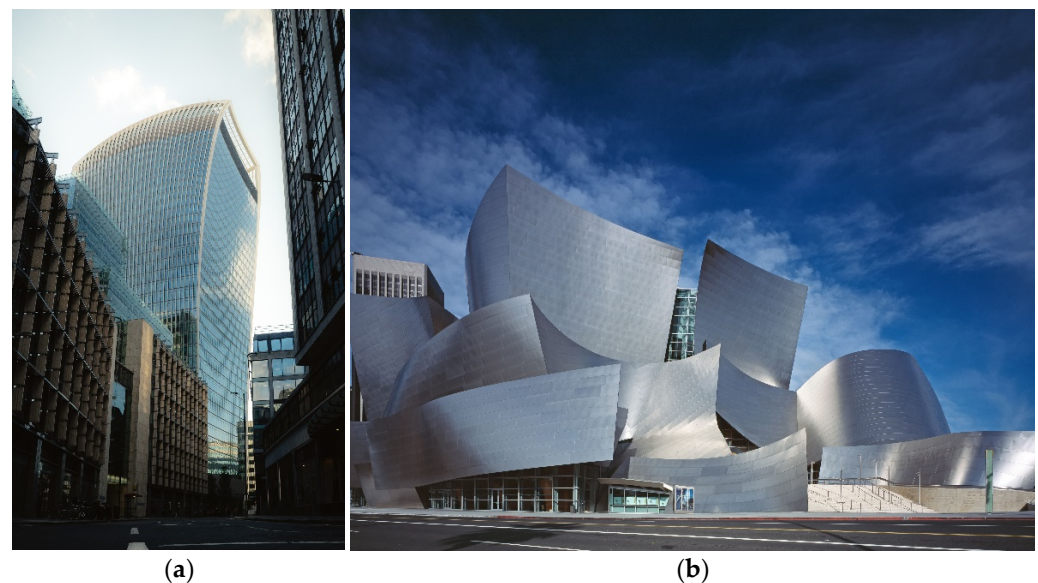


Figure 1. (a) “Walkie-Talkie” Building, London, UK [25]. (b) Walt Disney Concert Hall, Los Angeles, USA [25].

Table 1. Comparative analysis of the cited buildings.

Name of the Building	Façade Material	Building Geometry	Effects on the Surroundings	Mitigation Strategies Applied
20 Fenchurch Street-London, UK (Figure 1a)	Laminated glazing	Concave, single curvature	Reported focused solar radiation spot at pedestrian level six times higher than direct sunlight	External fins and shading systems
Vdara Building-Las Vegas, USA	Reflective glazing	Concave, single curvature	Reported raised temperatures in the surrounding areas and sunburns on pedestrian bystanders	Application of nonreflective solar films on the façade
Walt Disney Concert Hall-Los Angeles, USA (Figure 1b)	Stainless steel panels	Multiple double curvature surfaces	Multiple disabling glare sources, melted asphalt pavements due to the concentrated sunlight	Diffuse and satin-finishing of surfaces

A further representative example is the Walt Disney Concert Hall in Los Angeles (Figure 1b, Table 1), in which the freeform façade cladding in polished metal was responsible for glare and concentrated solar radiation phenomena. The latter caused the asphalt-covered pavement around the building to melt. A measurement campaign for temperature monitoring around the building recorded a 150 °C temperature over a piece of painted black foam core blackboard used as a reference absorber [19].

Concentrated irradiance is reported as a source of possible damage for all plastic or temperature-sensitive surfaces, which may experience localized melting or burns [26]. As a reference, we report that a minimum value of 8000 W/m² and 10 min of continuous exposure is needed to ignite common combustible materials, although autoignition is possible, depending on the material, only for values between 16,000 and 25,000 W/m² [27]. User comfort boundaries are included under lower values of the irradiance threshold. For short term exposures, but longer than the safe exposure time limit, which is 10 min, a radiation exposure of 1500 W/m² is considered a source of strong thermal discomfort. On the other hand, 2500 W/m² is considered the maximum value for people’s safety [28] with a maximum exposure of 30 s [28]. The presence of clothing can contribute to mitigating

this effect by allowing higher exposures times. A secondary effect related to the user's experience of the space, the risk of accidental damage due to direct contact with individual urban surfaces increases as their general or localized temperature increases.

Only a few cities have implemented measures that are prescriptive for the reflectance properties of the building surfaces. The city of Sydney applies a limit of 20% maximum reflectance for all the façade materials [29], and the same limit is implemented by the city of Hong Kong [30]. The planning strategies [31] mainly focus on reducing glazing areas or reshaping the texture of building surfaces to avoid any interference with the surroundings. In the literature, different approaches were tested to provide an adequate assessment of the effect of the solar radiation at the local and urban scale, but at present, there are no universally accepted criteria for the assessment of the maximum tolerance for reflected solar radiation affecting urban areas [28]. An experimental campaign aiming at testing the response of users exposed to glare found that users tend to be more tolerant to visually uncomfortable scenes while resting in an outdoor environment and performing no task or simple tasks, such as reading. Under these conditions, the subjects evaluated the glare conditions between perceptible and disturbing [32].

Reflected sunlight is in some ways unexpected due to its dependency on a scenario that is generally complex and the additional strict dependency on building geometry [33]. The definition of the right-angular optical properties of the involved surfaces [32] is also critical. The general approach leads to simulations created with dedicated software, but the results are unreliable when the accuracy of the surroundings, or of the building model itself, is not adequate.

Typically, simulations are performed during the early design stages, considering only the building masses and overlooking the presence of some façade details. Simplifications of the model are generally performed to retain simulation times within a limit of acceptability. How the building and its surroundings are simplified can strongly affect the results [34].

Raytracing methods can be used for caustics evaluation and identification of the Reflection Glare Area (RGA) [35]. The main limitation of the computational approach lies in the computing power and the level of detail requested for the model [36]. Custom-made tools are a solution to effectively include the geometry of the buildings and the optical reflectance properties of the material through the use of bidirectional reflectance distribution functions (BRDF) [22].

Experimental procedures refer to direct analysis of the scenario with High Dynamic Range (HDR) imaging of samples of exterior glare and a post-process digital analysis through a bespoke MATLAB tool [32] to identify glare sources within the context. Some other researchers have tested scale models of buildings with standardized geometries and surface materials able to redirect or concentrate the solar radiation. This is the case in [37], which tested cylindrical, concave, and triangular glass curtain walls, assessing the peak shift and the intensity of the solar radiation on their surroundings due to the building geometry.

The Boundary Reflection Area (BRA) was already proposed as a performance index for the reflection glare [38]. This approach neglects the reflectance of the building surfaces but identifies the type and the possible dimension of the region over which the reflected radiation impacts. This region, as an example of a standard test cubic building, presents a characteristic butterfly shape. All the reflections occur with the movement of the sun at the horizon. A forward-sloping façade between 10° and 20° can reduce the BRA, but determines an increase in the possible sun positions that can cause glare.

Other experiments were conducted with pure reflective surfaces resembling concave building geometries, trying to understand the effect of different parameters on the caustics. The variables considered in this study were building height, width, the radius of curvature, orientation, sun elevation, and azimuth angles [39]. The research aimed to test mathematical correlations, derived from optics, with simulations using precision software [40,41] and scale models [39].

However, as the critical review by Danks et al. evidenced [28], most of the literature focused on glare issues and general visual comfort [32,42,43], with limited investigation of the solar irradiance levels at the pedestrian level in front of tall buildings. While measurements have been performed for some case studies, these were usually carried out for a single building, without comparison between different design scenarios. A comprehensive raytracing modelling campaign by Wong assessed different buildings, but did not consider some of the geometries that lead to solar concentration [44].

Additionally, numerical modelling techniques are still in need of improvement [27], probably due to issues in the representation of the diffuse fraction of solar radiation in raytracing models, angular properties of materials, or a combination of these factors.

Yet, no systematic study compares the influence of building shape and material beyond some modelling attempts that require validation.

It is therefore important to provide the designers with a clear overview of the problem and its intensity in a way that prevents general errors during the early design stages and guides a detailed analysis that will reduce the risk of future local environmental problems that can lead to extra costs after the construction [45]. Therefore, the objectives of this research are to:

- (i) quantify the solar concentration (expressed in units of sun or suns) at the pedestrian level in front of archetypes of tall buildings with diffuse and specular reflective facades;
- (ii) identify the archetypes at risk of causing excessive solar concentration and harming pedestrians; and
- (iii) devise a measurement protocol that can be used to quantify shortwave radiative impacts (and solar concentrations) in real buildings, to assist in the identification of the need for façade retrofits and dispute resolution.

2. Methodology

This paper presents the measurement process and the results obtained during the experimental campaign carried out in order to investigate the effects of reflections due to sunlight for three standardized types of skyscrapers' geometries with two different façade finishings. The cases studied have been defined based on the preliminary review carried out.

The three geometries identified as representative typologies are:

- Vertical planar façade;
- Planar façade with 10% of vertical tilt;
- Curved concave façade (with a curvature radius of 60 meters, rescaled then at model scale).

In addition to the geometries, two façade finishings were analyzed which represented two possible extreme (worst- and best-case scenario) behaviors (detailed description in Section 3.1): specular and scattering.

2.1. The On-Site Measurements

2.1.1. Experimental Scenario

The experimental tests were carried out in Milan, Italy (45°28'45.713" North–9°13'47.937" East, 121 m above mean sea level) on an unobstructed rooftop of a university building, equipped with a complete weather and radiometric station.

The experimental set-up consisted of a 6 m × 1.5 m (Figure 2) grey coated work plane placed at 1 m height (over the building roof). The dimension of the plane and optimal measurement grid was defined using preliminary hourly simulations (with Rhinoceros 5.0 [46] and Grasshopper [47]), considering forward raytracing algorithms and Fresnel geometrical reflections. The grey matte base (albedo = 0.36) was selected for the plane as a representative mean reflectance of urban albedo.

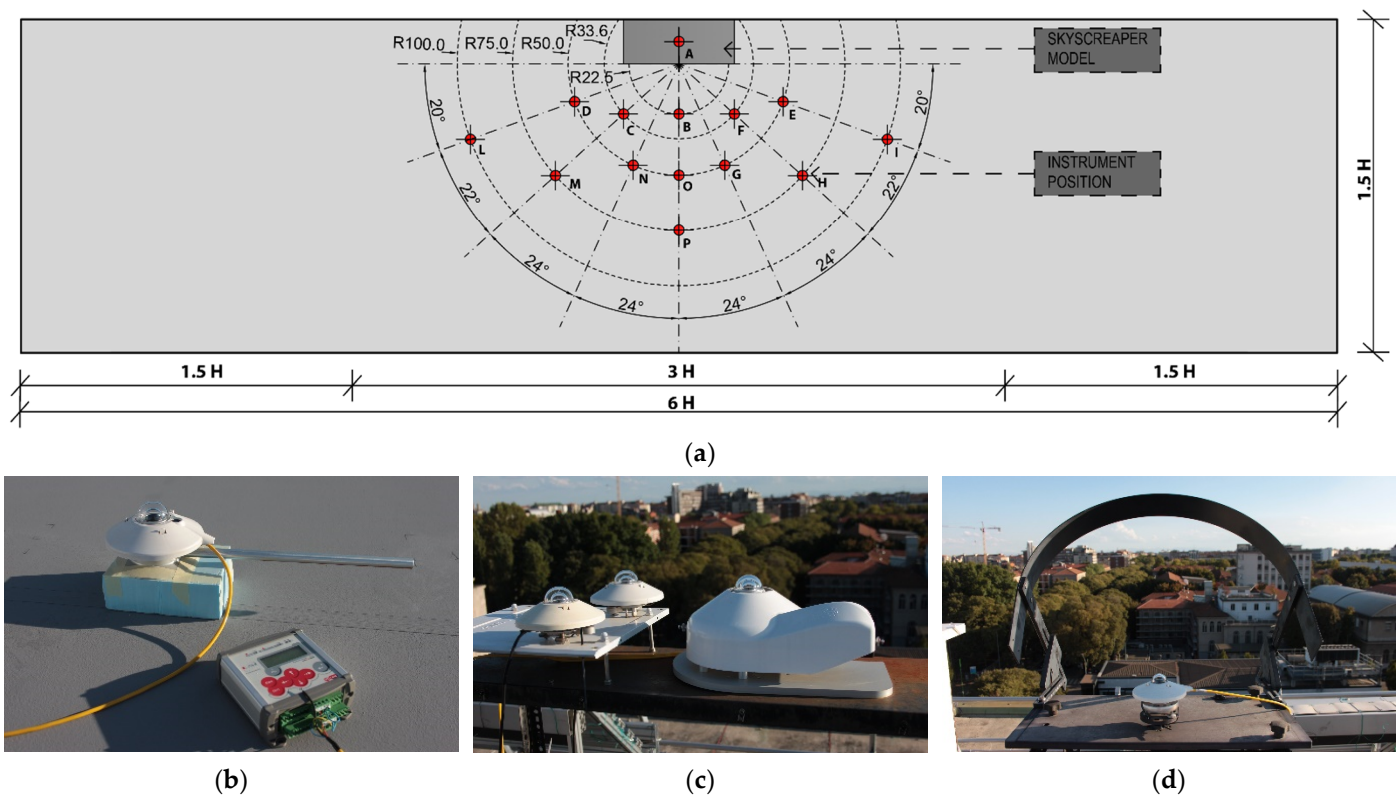


Figure 2. (a) $6 H \times 1.5 H$ measurement plane (H is the height of the Skyscraper model that in the presented experiment is equal to 1 m) with measurement positions. (b) Moveable albedometer (CMA11) with Datalogger. (c) Pyranometer CM21 and CM22 are part of the weather station that provides undisturbed reference values. (d) Pyranometer CM6 with shadow-band that provides undisturbed reference values.

Based on the results obtained from the preliminary analysis, the positions of the measurement points were defined with a double construction: the points were placed in the intersection between a radial subdivision (relatively 20° and 22° in the external part and 24° in the central part) over a circumferential construction (relatively with a radius of 100 cm, 75 cm, 50 cm, 33.6 cm, 22.5 cm), as shown in Figure 2. This approach allowed the identification of the behavior of both diffuse and specular reflectors for the three geometries. Furthermore, this configuration allowed the evaluation of the impact of the façade on possible relevant context areas close to the building model, such as squares, streets, and adjacent buildings.

2.1.2. Scale Models

In order to assess the increment of solar radiation generated by tall building solar reflection, three skyscraper scale models were built based on a review of contemporary skyscraper dimensions and shapes [35,41,45,48].

The 1:100 scale models were $20 \times 50 \times 100$ cm parallelepiped-shaped wood structures with white diffusive finishing, except for the front façade surface which could be replaced according to the required analysis. Other authors have proposed another similar reference model in a virtual scenario [35], where four buildings (with concave, convex, angular, and planar geometries) with a façade dimension of 100×40 m were considered representative (Figure 3).

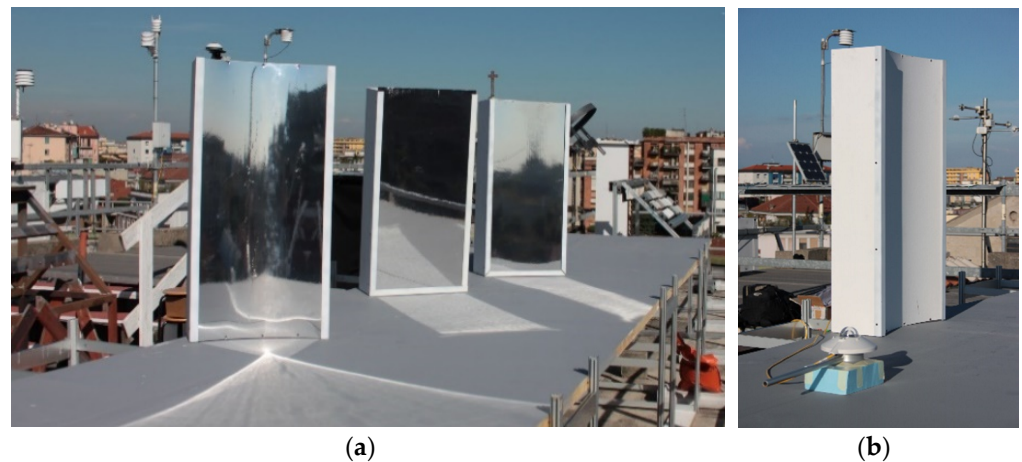


Figure 3. (a) Three skyscraper scale models with reflective film as a finishing surface. (b) Concave skyscraper scale model with white scattered film as a finishing surface.

Two finishing materials were selected for the front changeable façade: a white scattering diffusing surface and a specular reflective material, which are representative of the extreme cases in façade applications.

These case study geometries permitted the investigation of the reflection phenomenon, during a clear summer day, for three characteristic tall building shapes.

2.2. Experimental Sample Material Properties

To identify the adequate façade diffusive and specular materials for the tests, different white finishing paints and mirror films were measured to find their relative spectral reflectance values. Two of them with similar solar reflectance values were selected for the experiment to ensure the differences were due to variations in their optical angular behavior and not in their total reflectance. A Perkin Elmer Lambda 950 Spectrometer was used (for wavelengths between 250 and 2500 nm) according to UNI 14500 [49], and the values were post-processed following the ASTM E903 [50] procedure. Figure 4 shows the results of the measurement procedure for the selected materials used during the experimental campaign.

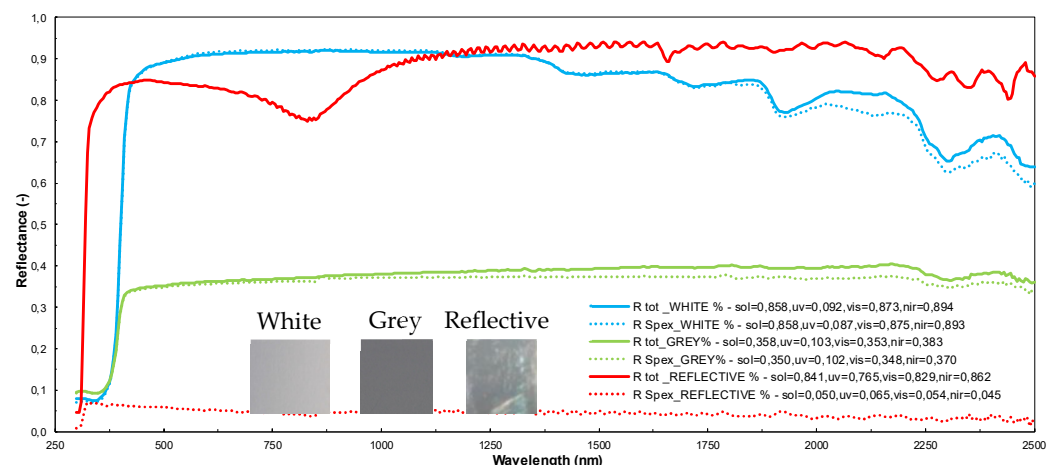


Figure 4. Spectral and computed solar (sol), UV, visible (vis), and near-infrared (nir) reflectance of the diffusive materials and specular film. The measurements are repeated for total (R tot) and specularity-excluded (R Spex) reflectance.

As a scattering diffuse surface (Figure 4, blue line), a typical white painting with a solar reflectance equal to 0.86 was chosen. It showed a typical spectral curve of light-diffusive materials. The specular surface selected was a metallized mirror-like (especially for high-

reflectance angles) polyester film (Figure 4, red line) that had a mean of 0.85 as its solar reflectance value. From a preliminary qualitative analysis, not having the possibility to perform complete BRDF for the material under analysis through the comparison of the reflectance curves (total and specular excluded), we can say that the specular component remains predominant regardless of the angle of incidence, although we cannot state this with certainty.

With the aim of preliminarily evaluating if the mirror film is perfectly reflective, the specular excluded reflectance was measured. Analyzing the obtained results, it is possible to highlight that 95% of solar reflectance is due to a specular component. Both finishing materials presented almost the same integral value of solar reflectance, and the choice was intentional to compare the results of solar radiation insisting on the surroundings under different reflective behavior of the building models.

Figure 4 also shows both total and specular excluded reflectance of the background plane used. This grey surface was selected because it represents the standard urban surface with an albedo of 0.35 [51–53].

Instruments and Measurements Procedure

Three different sets of instruments (some of which were from the weather station placed next to the measurement site) were used:

- An albedometer (CMA11 by Kipp & Zonen), with data recorded by an M-Log logger (by LSI) placed over a specific plastic support, was used to measure solar irradiance in different positions over the test plane (Figure 2b). The CMA11 is a secondary standard albedometer with a maximum solar irradiance value equal to 4000 W/m^2 and 5 s of response time.
- CM21 and CM22 pyranometers (by Kipp Zonen) were used to measure the undisturbed solar irradiance and calibrate the albedometer.
- A CM6 pyranometer with a shadow-band was used to measure the diffuse component of solar radiation.
- A thermal infrared camera was used to verify the temperature increase on the plane due to reflections.

All the measurements were carried out in one week in order to have similar sun position and radiation values. The survey was performed during a typical Italian summer clear-sky day, from the 19 to the 25 of September, during the daylight hours from 9 a.m. to 6 p.m. with a maximum solar elevation of 46.04° . The measurements were taken under equal solar diffuse fraction, namely with the same diffuse/global ratio during the same hour.

The Unit of Sun (UoS) was defined as a normalized value describing the ratio of the reflected irradiance over the ambient solar irradiance measured on the horizontal surface on the top of the scaled building mock-up, as defined in [34].

A total of 54 scenarios were measured, combining the three building geometries with the two previously described alternatives for the façade finishing material.

During each measurement session, the solar irradiance values in the 14 points over the plane were measured, moving the albedometer every minute (so that the measurement readings could be considered as stable) and over each position. Data acquisition time depended on the instrument response time lag and sky conditions. The measurement sequence, named with progressive letters; start from the acquisition of undisturbed solar radiation (above the skyscraper), passing through the points over the measurement plane and concluding with a vertical solar irradiance. All the geometries and materials have been analyzed with the same procedure, as previously explained. All the recorded values were compared with the ones gathered from a reference weather station located on the same floor of the measurement plane.

2.3. The Simulations Workflow

2.3.1. The Façade Material Benchmark

The optical performance of glass is typically angular; namely, it depends on the angle of incidence of radiation that hits the surface. In general, and for incidence angles $\alpha < 60\text{--}70^\circ$, the visible solar transmittance of a single or double glass is close to the value measured for a normal incidence ($\alpha = 0^\circ$). For angles of incidence above this threshold, the transmittance value decreases, while the reflectance increases exponentially.

In order to understand how representative the choice of a highly reflective finishing was for our building model, the yearly high solar reflectance behavior of a typical glazing façade made with a Double-Glazed Unit (DGU) was evaluated.

Two types of glass were selected to describe two common DGUs that could be installed in a new skyscraper building in accordance with its optical and energy needs (Table 2). The two selected materials also allowed us to evaluate the extreme behaviors that could include all the possible causes related to intermediate properties of systems and components. The selected DGUs included one with high reflectance and solar control properties, penalizing light transmission properties, and a second DGU with good solar control values and a high selectivity index.

Table 2. Solar and visual properties of the Double-Glazed Units (DGUs) selected as a reference for our analysis, considering solar transmission (τ_s), solar reflectance (ρ_s), and visual transmittance (τ_v).

Description	Code	τ_s [%]	ρ_s [%]	τ_v [%]
High Reflective Sun Control_DGU	HR_SunC	9.9	53.3	15.1
Selective_DGU	SEL	31.6	23.9	66.5

In Figure 5, the angular solar transmittance and reflectance properties are reported for the DGUs listed in Table 2. The values were computed using LBNL WINDOW 7.7 [54]. The normal reflectance value of the HR_SunC case was approximately twice that measured for the Selective (SEL) DGU. For high incidence angle of solar radiation (i.e., $>70^\circ$), the percentage increases of the reflectance of the two analyzed DGU types are comparable, regardless of whether the two measured reflectance values at normal incidence (ρ_s) are very different.

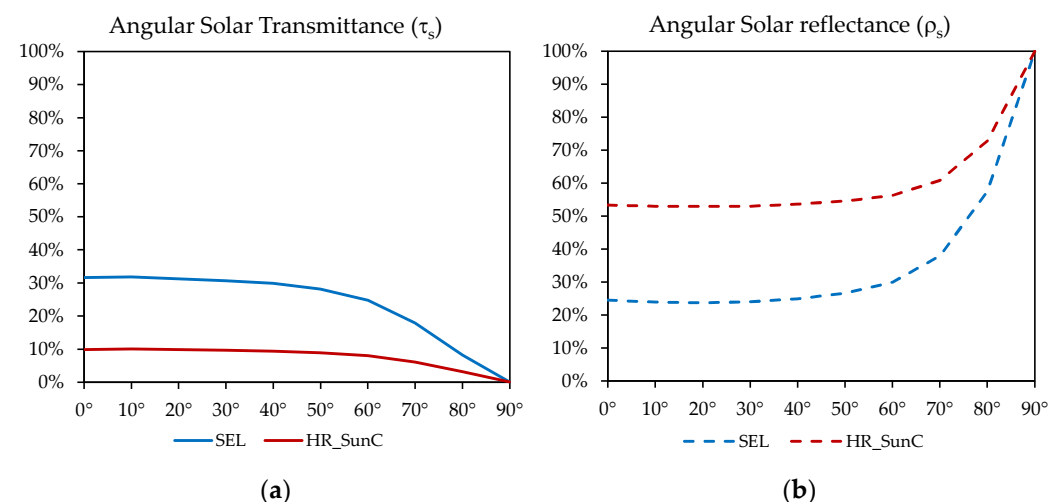


Figure 5. Angular solar transmittance— τ_s (a) and angular solar reflectance properties— ρ_s (b) of a selective (SEL) and High Reflective Sun control (HR_SunC) double glass unit. On the x-axis, the incidence angle α is reported.

2.3.2. A Parametric Analysis Script for Unwanted Reflections of a Glazed Façade

Regarding the above considerations (Section 2.3.1) on the variation of the optical performance of transparent systems, a parametric script was developed in Rhinoceros

5 [46] within the Grasshopper [47] environment to evaluate the probability of occurrences of unwanted solar reflection phenomena for a generic curtain wall surface. The script considered: the variability of the site (latitude/longitude); the orientation of the building masses; and the slope of the surfaces [55].

The script considered the solar rays as vectors to reduce calculation time, allowing a comprehension of the number of rays that hit the surface. The script was based on the following hypotheses:

- Every “solar ray” represents the sun’s position in the middle of each sun hour of radiation;
- A quad mesh subdivision of the building mass surface was used in order to replicate a realistic building façade panelization, made through the use of discrete glazed elements.

The working flow proposed (Figure 6) lists the incident solar rays coupled with the related normal vector of every mesh tile. This approach allowed the script to correlate the initial vector list with the angular degree, excluding (by the use of filters) the portion of rays not required, based on the designer criteria.

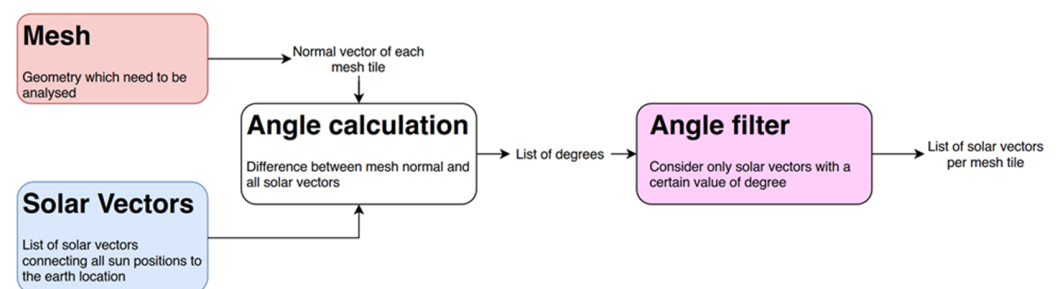


Figure 6. Grasshopper script workflow.

The parametric model defined is capable of parsing sunrays incidence angles based on their inclination for each surface normal vector. The system creates a virtual circular radiation cone (Figure 7a), with its vertex on the surface’s central point and a perpendicular orientation to the face.

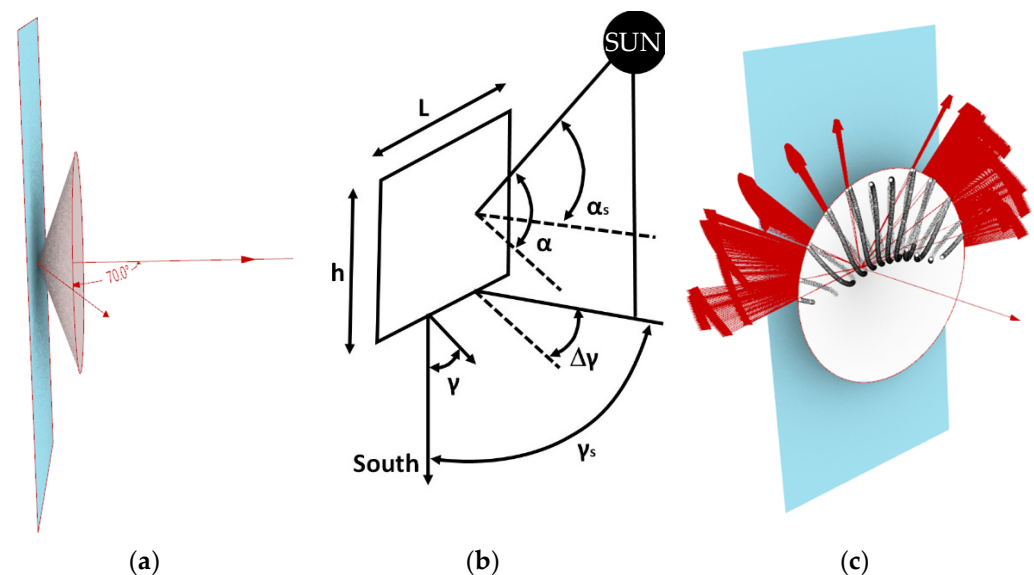


Figure 7. (a) The extent of the radiation cone that has a lower probability of creating unwanted solar reflections. (b) The model for evaluating the incidence solar radiation angle. (c) Representation with, highlighted in red, the hourly annual solar positions that have the maximum probability of creating unwanted reflections.

Such geometry allows the control of the cone angle by increasing or reducing the number of rays hitting the surface beyond a certain degree. As shown in Figure 5, an angle

between 70° and 90° could generate reflected radiation on the surroundings. Considering this, the scripts can directly provide the number of hours over the entire year in which a mesh tile has this behavior (Figure 7c).

For every mesh tile, a virtual circular cone of a certain amplitude, based on the glass properties, was created in its center. The cone represents the solar rays filter; in this way, it is possible to visualize the number of vectors between 90° (the tile plane) and the angle α of the cone.

The generic incidence angle of the solar radiation over the surface was evaluated in accordance with [56], using the following equation (based on Figure 7b):

$$\tan(\alpha) = \frac{\tan(\alpha_s)}{\cos(\Delta\gamma)}$$

where:

- (α) is the incidence angle;
- (α_s) is the hourly solar altitude; and
- $(\Delta\gamma)$ is the difference between the hourly solar azimuth (γ_s) and the azimuth of the surface normal (γ), both measured from the South.

Based on the geographical location and orientation of each mesh, the script can evaluate the entire spatial distribution of solar rays hitting the interested surfaces over a year. Complex façade geometries and double-curved envelopes can potentially create over-shadowing effects, hiding a façade portion from solar rays, because of the coverage of part of the sky vault.

The parametric script (Figure 8) provides a double filter level which excludes from the analysis all the rays screened by the obstructions and the ones out of the portion of the skydome seen by each analyzed surface. Once the filtering has been performed, it is possible to retrieve the amount of the reflected radiation by using the radiation cone.

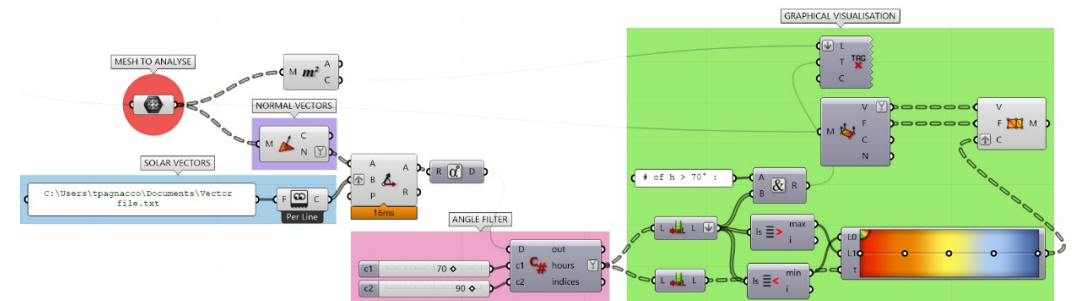


Figure 8. Example of the parametric script developed in grasshopper.

3. Results

3.1. Experimental Measurements

The experimental measurement presented in the following section is a part of the entire measurement campaign carried out and completely reported in Appendices A–F. In order to present the recorded value in a comparable way the undisturbed values recorded by the weather station will be taken as reference.

The 25th of September had almost a completely clear sky condition; during the other two days, some atmospheric turbidity was present in the central part of the day (Figure 9b).

Tables 3 and 4 and Appendices A–F include all the irradiance values recorded for the registered interval and for the points that were selected as representatives to describe the magnitude of the solar radiation over the surroundings of each model.

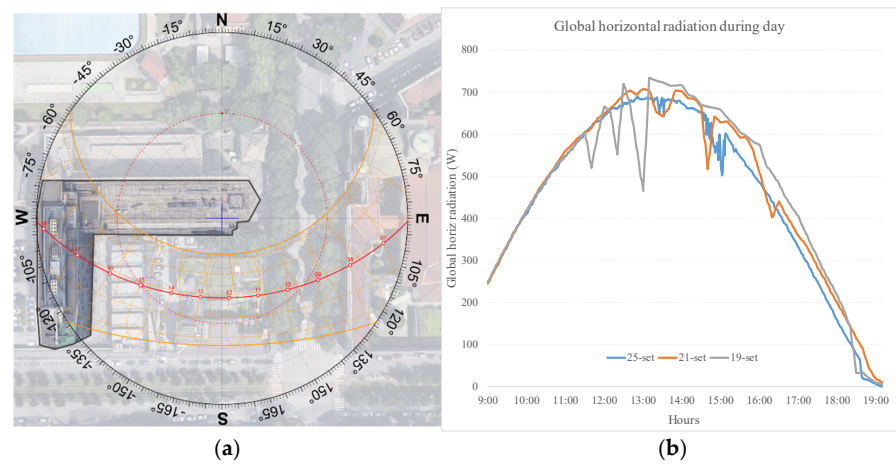


Figure 9. (a) Test site plan view (Politecnico di Milano, Nave Building) with September sun path. (b) Global horizontal radiation during test days (19, 21 and 25 September).

Table 3. Reflection for flat façade models: preliminary analysis and measurement results for 10:00, 13:00, and 16:00. For each point and in bold: the measured value (Meas.), the non-disturbed measure (N.d.Meas), the Unit of Sun (UoS), and the time (Time) of the measure. All the measurements are shown in Appendix B. In grey the measurements points within the solar reflection area.

		Flat Reflective Façade			
		Meas. [W/m ²]	N.d.Meas [W/m ²]	UoS [-]	Time [hh:mm]
h. 10:00	A	406	410	0.99	10:00
	B	422	413	1.02	10:01
	C	754	416	1.81	10:02
	D	431	420	1.03	10:03
	E	467	422	1.11	10:04
	F	445	424	1.05	10:05
	G	444	424	1.05	10:05
	H	450	428	1.05	10:06
	I	458	428	1.07	10:06
	L	439	431	1.02	10:07
	M	870	434	2.00	10:09
	N	441	439	1.01	10:10
	O	438	442	0.99	10:11
	P	437	446	0.98	10:12
h. 13:00	A	693	686	1.01	13:06
	B	1321	687	1.92	13:07
	C	705	685	1.03	13:08
	D	698	685	1.02	13:09
	E	694	685	1.01	13:10
	F	708	684	1.03	13:11
	G	711	684	1.04	13:12
	H	691	685	1.01	13:13
	I	697	686	1.02	13:14
	L	686	681	1.01	13:15
	M	685	676	1.01	13:16
	N	704	676	1.04	13:17
	O	1327	683	1.94	13:18
	P	1374	684	2.01	13:19

Table 3. Cont.

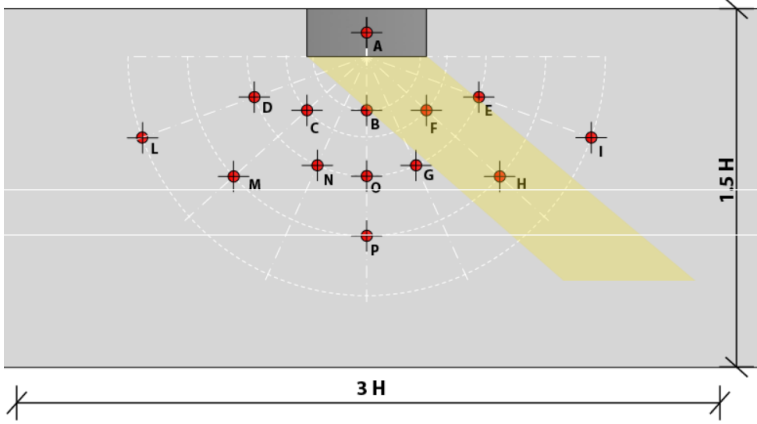
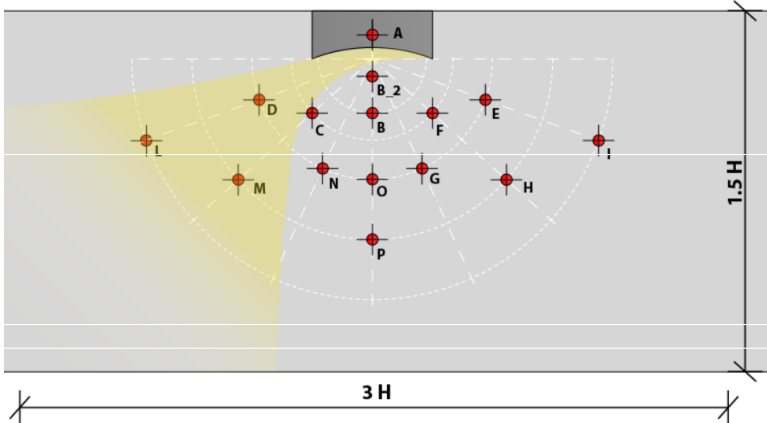
Flat Reflective Façade					
h. 16:00		Meas. [W/m ²]	N.d.Meas [W/m ²]	UoS [-]	Time [hh:mm]
		A	462	456	1.01
B	481	452	1.06	16:15	
C	468	452	1.04	16:15	
D	486	449	1.08	16:16	
E	455	449	1.01	16:16	
F	782	446	1.75	16:17	
G	428	441	0.97	16:19	
H	635	441	1.44	16:19	
I	453	439	1.03	16:20	
L	445	438	1.02	16:21	
M	442	434	1.02	16:22	
N	440	428	1.03	16:23	
O	440	428	1.03	16:23	
P	435	428	1.02	16:24	

Table 4. Reflection for curved façade models: preliminary analysis and measurement results at 10:00, 13:00, and 16:00. For each point and in bold: the measured value (Meas.), the non-disturbed measure (N.d.Meas), the Unit of Sun (UoS), and the time (Time) of the measure. B_2 was introduced to better characterize the reflection next to the façade. All the values are shown in Appendix F. In grey the measurements points within the solar reflection area.

Concave Reflective Façade					
h. 10:00		Meas. [W/m ²]	N.d.Meas [W/m ²]	UoS [-]	Time [hh:mm]
		A	341	350	0.98
B	370	365	1.01	9:40	
B_2	375	367	1.02	9:41	
C	394	367	1.07	9:41	
D	450	371	1.21	9:42	
E	419	374	1.12	9:43	
F	396	377	1.05	9:44	
G	395	377	1.05	9:44	
H	404	379	1.07	9:45	
I	409	381	1.07	9:46	
L	422	383	1.10	9:47	
M	464	386	1.20	9:48	
N	389	388	1.00	9:49	
O	386	390	0.99	9:50	
P	384	390	0.99	9:50	

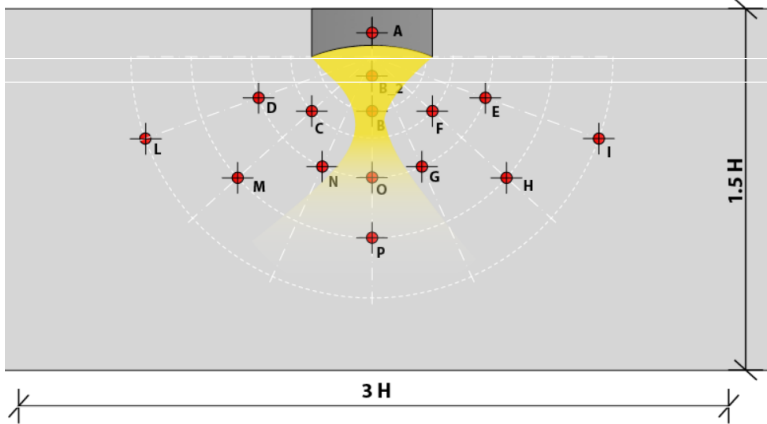
h. 13:00		Meas. [W/m ²]	N.d.Meas [W/m ²]	UoS [-]	Time [hh:mm]
		A	689	678	1.02
B	1286	677	1.90	12:43	
B_2	1521	678	2.24	12:44	
C	696	678	1.03	0:00	
D	680	677	1.00	12:45	
E	694	679	1.02	12:46	
F	701	683	1.03	12:48	
G	702	684	1.03	12:49	
H	696	686	1.01	12:50	
I	713	689	1.03	12:51	
L	701	688	1.02	12:52	
M	687	684	1.00	12:53	
N	718	684	1.05	12:54	
O	1103	683	1.62	12:55	
P	812	683	1.19	12:56	

Table 4. Cont.

Concave Reflective Façade					
h. 16:00	Meas. [W/m^2]	N.d.Meas	UoS	Time	
		[W/m^2]	[-]	[hh:mm]	
	A	547	533	1.03	15:37
	B	554	530	1.05	15:38
	B_2	557	530	1.05	15:38
	C	540	524	1.03	15:39
	D	557	524	1.06	15:39
	E	719	524	1.37	15:40
	F	1237	524	2.36	15:40
	G	522	523	1.00	15:41
	H	653	523	1.25	15:41
	I	571	522	1.09	15:42
	L	534	522	1.02	15:42
	M	531	519	1.02	15:43
	N	531	519	1.02	15:43
	O	533	518	1.03	15:44
	P	527	517	1.02	15:45

Experimental measurements showed a significant increase in solar irradiance values due to solar reflection, both for specular and scattered materials. For all the geometries, the irradiance values were strictly connected with the façade shape and measurement position. With the white scattering surface, it is possible to notice an overall increase in solar irradiance depending on the distance between the measurement point and the scale models. No significant variations were observed with a change in the geometries of the building models, meaning that for the scattering material, the only significant variable is the distance from the façade.

The analysis of the specular reflective surface showed a completely different pattern. Indeed, outside the reflection area, all the geometries show values equal to the undisturbed one, while inside the reflected area the values recorded are up to five times greater than the solar radiation on the horizontal plane (façade with a concave geometry presented in Table 4).

Considering the concave surface, this unique building geometry concentrates the reflected sunlight in a small focal point characterized by a strong increase of perceived light (Table 4) and of surface temperature intensity, which can only be estimated due to the nature of the urban environment that is also influenced by the surface's thermal mass, solar absorbance, and emissivity, such as transient local parameters (such as wind velocity and water presence, as in [28,34]).

Indeed, for the flat and 10% tilted façade, the values doubled the undisturbed solar irradiance for the concave shape. This was due to the Fresnel effect on light reflections, which is greater than five times in the focal point (no precise value has been measured, as it was higher than the full scale of the Table 4. For this reason, Tables 3 and 4 show the results obtained for the flat reflective and the concave reflective façades in three parts of the day.

Compared to scattering material, where the solar irradiance curves at ground level and presents a flat upward shift with respect to horizontal irradiance, for high specular material, it is possible to notice peaks depending on the measurement points and solar position. For the flat reflective façade and in every analyzed position (Figure 2a), a peak value between 1200–1350 W/m^2 was reached during different hours of the day, and a result was obtained that is two times more than the measured horizontal irradiance (Table 3).

Curved façades behave like a solar concentrator, generating reflection tracks and high irradiance values on the ground. Inside the reflection path, the irradiance values exceed 40–60% of the undisturbed radiation values, while on the shape edges it is possible to reach 100–130% higher irradiance values. The critical area for collector shapes is the focus; near the focus the irradiance value can reach 1800–2200 W/m^2 compared to the global horizontal irradiance of 650–700 W/m^2 . Inside the focus, values higher than 3000 W/m^2 have been

reached, and at noon, the instrument limit (4000 W/m^2) was overtaken, implying that it reached values far above this threshold. Table 4 shows different light-track geometries and the respective recorded values for each measurement position.

Figure 10 shows a comparison, assuming the same type of façade (flat) and same measurement position, between the scattered and the specular façade materials. In Figure 10a, it is possible to see that during the day, the increase of reflectance of the scattering material is affected by the distance from the façade. However, in Figure 10b, it is possible to see that regarding the specular material, when the measurement point is inside the reflected area there is twice the irradiance. When outside, the values are the same as those of the undisturbed one.

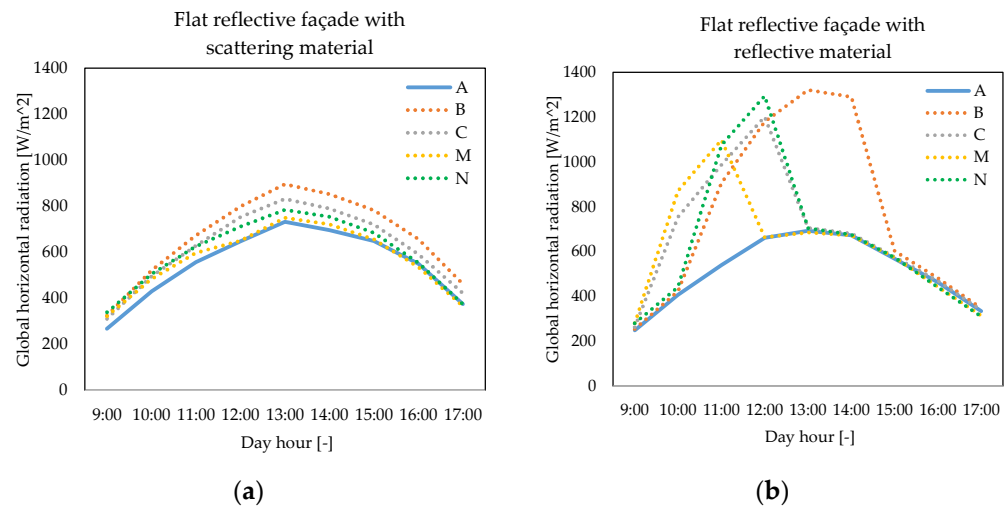


Figure 10. Time-dependency value of solar radiation for five measurement points (A, B, C, M, N) for scattering (a) and specular (b) planar façade geometry (21 September).

The use of the selected light-diffusing material shows radiation values constantly increasing in all the directions around the building model with an intensity that changes only in relation to the distance from the façade (the measured peak is $\sim 133\%$ at 15 cm distance from the façade, equivalent to a H/D ratio of 6.66 in a real building scenario and in which D is the Distance from the façade and H the Height).

Regarding the reflective materials, the behavior of the three geometries is completely different. For the flat geometry, the value of solar irradiance in the reflected area reached a peak of $\sim 200\%$; while outside of the “reflection zone”, the values were almost similar to the irradiance measured on the horizontal plane. The curved façade can have an easy prediction of the caustic shape. The curvature of the façade itself must be adequately large to reduce the intensity of the solar radiation in the focal point, otherwise, the extent of the reflective or specularly reflective façade material should be reduced. The behavior of the 10% tilted flat geometry is similar to that of the flat vertical one, with a similar shape of the reflected area, but with less extension from the building façade (due to its 10% inclination) and radiation values inside that are slightly higher. The convex curved geometry produced a focal point in which the solar irradiance reached values higher than $\sim 300\%$.

Some authors [57] suggest the use of alternate finishings on the façade, or different materials to avoid reflections problems over the pedestrians. A standard geometry building facing an urban canyon was considered as the reference example. In this case, the use of reflective materials under the fourth floor was discouraged, while the use of retro-reflective or purely diffuse materials was suggested.

A further measurement carried out was thermography. Thanks to these measurements, it was possible to indirectly identify the temperature reached by the surface (with the grey coating shown in Figure 4) due to reflection. With this approach, it is also possible to identify the behavior of the concave façade from a quantitative point of view, as shown in Figure 11. In the focus of the parabola, describing the geometry of the parabolic façade,

a severe concentration of solar radiation is present, but on a very limited portion of the surrounding plane. A zone in which the surface temperature considerably exceeds the reference of the temperature scale, set at 100 °C, is clearly identifiable. The distribution of temperatures in the other cases examined is uniform over a larger area of reflection and with values between 60 and 80 °C. The surface temperature results for the curved vertical façade are comparable with the literature findings.

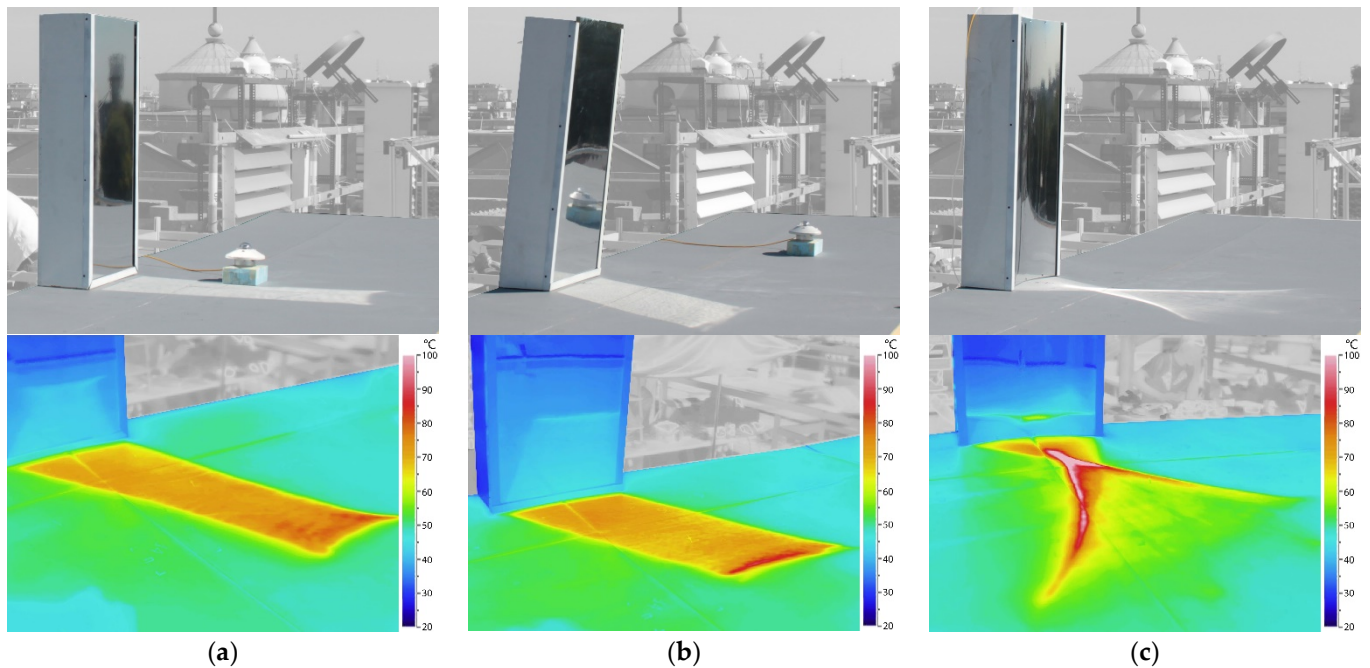


Figure 11. (a) The reflection shapes (photo on the top and thermography on the bottom) of the skyscraper scale model with a flat vertical façade coated by the reflective film. (b) The reflection shapes (photo on the top and thermography on the bottom) of the skyscraper scale model with a flat 10% tilted façade coated by the reflective film. (c) The reflection shapes (photo on the top and thermography on the bottom) of the skyscraper scale model with a curved vertical façade coated by the reflective film.

3.2. Simulated Frequency Distribution of Solar Reflection Occurrences: Hourly Annual Distribution

Among the results of the preliminary assessment of the building masses, and obtainable through the developed script, it is possible to derive a temporal evaluation of the hours and days during the year in which a generic façade glazed tile and part of the façade meshes are likely to be subject to phenomena of reflection and/or concentration of solar radiation. This can be considered a preliminary risk assessment that depends on geometry, latitude, longitude, and orientation. The following results are exemplificative of the potential risk of a glazed vertical façade module.

The analysis was carried out to determine all the possible angles of incidence of solar radiation that annually can insist on a building with a flat vertical façade facing South (S), East (E), or West (W), in addition to the two intermediate positions, South-East (SE) and South-West (SW). This model is representative of one of the test cases analyzed during the experimental campaign. This hourly analysis was developed considering the latitude and longitude of Milan.

A representative hourly annual distribution of the solar reflection occurrences is presented in Figure 12 for the South-exposed façade.

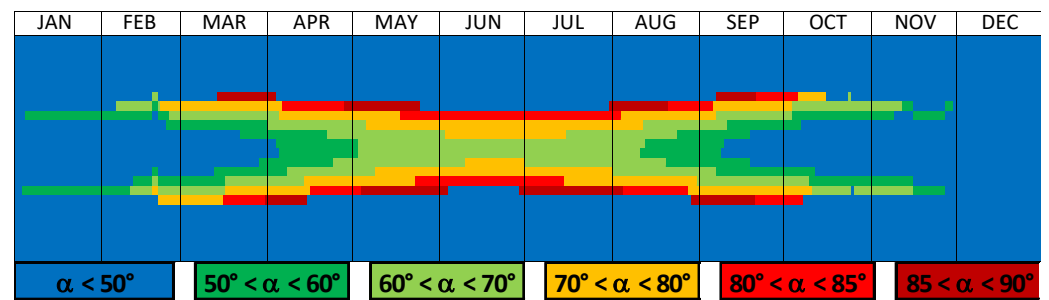


Figure 12. Annual hourly distribution of the incidence angles of the solar radiation over the façade of the classical vertical South-oriented skyscraper model.

In the following carpet graph, the different days of the month are reported on the x-Axis and the different hours of the day on the y-Axis. It is then possible to highlight that the first and the last hours of the day during the winter months are critical, and particular attention must be paid to the central hours of the day during the summer months when the incidence angles distributions are greater than 80°.

In general, we considered the 70° angle of radiation incidence as a threshold that could generate negative phenomena of concentrated reflection of solar radiation on the surrounding context. Since the façade of the building model considered is planar and vertical, it is possible to assume that each module of the façade, i.e., each portion of it, has a uniform and homogeneous behavior, respecting the previously identified rules for possible unwanted reflections.

Table 5 shows the incidence angle frequencies compared to the total number of hours of light during the year. The results show that the phenomenon is not negligible, since it afflicts the façade of the building between 22% and 28% of the time, in the same way. We note that the most critical exposure for this type of façade geometry is South, followed by the East (or West), and finally the couple SE/SW. Other façade geometries and alternative locations could lead to different distributions of the angles of incidence, increasing or decreasing the number of critical hours.

Table 5. Percentage of solar radiation incidence angles per orientation over the flat façade of the vertical building. The percentages are related only to sunlight hours.

Incidence Angle α of the Solar Radiation Per Orientation—Flat Vertical Façade			
α	E/W	SE/SW	S
$\alpha < 50^\circ$	51%	42%	34%
$50^\circ < \alpha < 60^\circ$	15%	22%	16%
$60^\circ < \alpha < 70^\circ$	11%	15%	21%
$70^\circ < \alpha < 80^\circ$	8%	11%	16%
$80^\circ < \alpha < 85^\circ$	10%	5%	7%
$85^\circ < \alpha < 90^\circ$	5%	5%	6%
Total > 70°	23%	21%	29%

3.3. Simulated Frequency Distribution of Solar Reflection Occurrences: Spatial Surface Distribution

In case of any complex façade surfaces, and for every single mesh, which describes the panelized surface of the generic building mass, the number of hours per year, or the possible occurrences of unwanted reflection, they can be represented using a false color scale. The model is simplified, not considering the solar deflection of the glass, which could modify or amplify the occurrence of the phenomenon.

Unlike the analysis presented in the previous section, it is not possible to know which hours and periods of the year unwanted reflections phenomena occur. However, it is possible to identify which portions of the building mass surface are characterized by the highest number of negative occurrences. The script, in this case, was therefore used as a

pre-assessment of the proposed geometry, favoring the designer's activity in suggesting possible variations to provide effective proposals for the modification of the geometry during the design phase or to provide local treatments to mitigate the effects.

Therefore, it is possible to make qualitative deductions comparable to the following:

- In the southern-exposed facades with parabolic sections, the possibility of negative effects becomes greater while moving away from the geometric focus of the parabola that describes the surface (Figure 13a);
- In the case of east-facing exposed parabolic surfaces, the area that is close to the focus of the parabola seems more critical (Figure 13b).

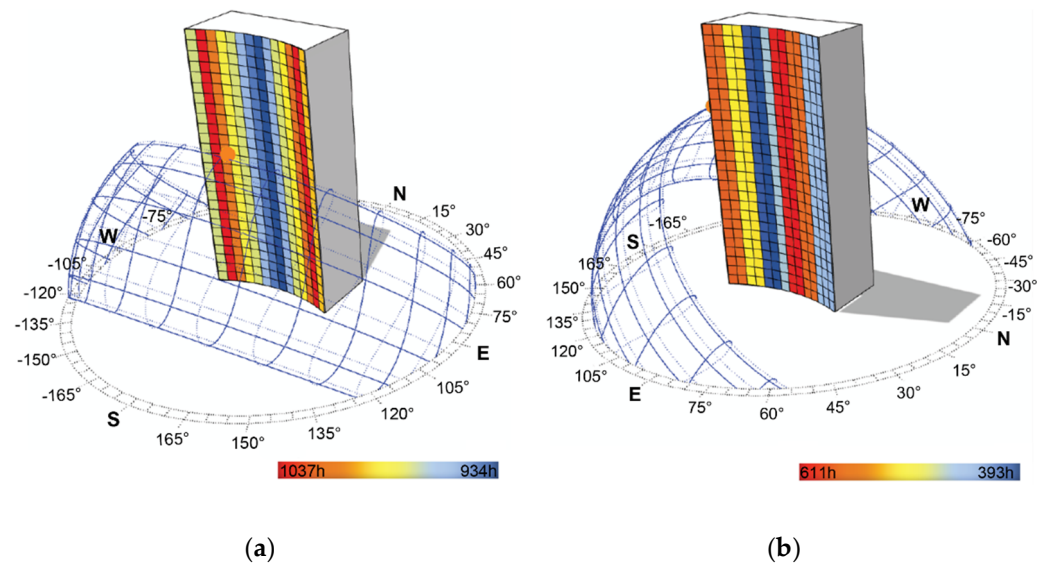


Figure 13. (a) Building mass with a parabolic façade facing South. (b) Building mass with a parabolic façade facing East. Both buildings are located in Milan.

Further developments will be the subject of analysis in future publications, in which the script will be expanded in its possibilities of use.

4. Discussion

Our results quantify the risk of solar concentration posed by buildings with specularly reflective facades, especially with a concave façade geometry facing the equator. A single high rise building with a flat diffusive façade with an albedo of 0.86 (i.e., an unsoiled white) causes an increase of the incident solar irradiance on the ground by a maximum of 20% (i.e., 1.2 suns at pedestrian level). This is still a significant increase, although the hardware model represents a worst-case scenario, without windows or overhangs.

As in [16], if we consider a building of indefinite length, we can compute the fraction of incident radiation that returns to the sky, which is 36% for a Lambertian wall and pavement with albedo equal to 0.60 and 0.20, respectively. In our case, the fraction of solar radiation returning to the sky was 58% [computed as $0.86 \text{ wall albedo} \times (0.5 \text{ sky view factor} + 0.5 \text{ ground view factor} \times 0.36 \text{ ground albedo})$]. Levinson et al. computed that a retro-reflective wall with albedo of 0.60 increases the solar radiation escaping the city to 55% (with a Lambertian street pavement with albedo = 0.20) [16].

Instead, the mirror-like finish, both in the flat and concave configuration, leads to peak irradiances reaching the ground, even three times the incoming irradiance (i.e., 3 suns). This does not approach the degree of solar concentration achieved by Fresnel reflectors designed for high concentration photovoltaics [58], which can exceed 1000 suns. However, local effects and some polished metal cladding might achieve higher values than those we measured, possibly approaching the 25–50 suns of the early developments in solar concentration PV [59]. Indeed, the façades of buildings might perform as modular Fresnel

lenses. Therefore, our results do not constitute a worst-case scenario, but rather a realistic scenario of downward reflection of solar radiation with a specularly reflective façade.

Some authors [57] suggest the use of alternate finishings on the façade, or different materials to avoid reflection problems for pedestrians. A standard geometry building facing an urban canyon was considered as the reference example. In this case, the use of reflective materials under the fourth floor was discouraged, while the use of retro-reflective or purely diffuse materials was suggested.

Retro-reflective materials have been proposed as a solution. However, like high-albedo materials [60], they are subject to ageing problems, which decrease their reflectance and retro-reflection over time. Their performance is almost fully recovered after cleaning only by prism-type retro-reflectors [61]. However, only a limited number of studies have been performed on the durability of retro-reflectors. Furthermore, retro-reflectors display the maximum upward to downward reflection ratios for low angles of incidence [62]. This may provide a positive performance at sunrise and sunset, but the retro-reflection ratio is limited to 30–50% during peak hours. Therefore, the application of retro-reflective materials cannot be a panacea for solving careless design. Much attention has been paid in the literature to the potential negative effects on thermal comfort of pedestrians that would be produced by high-albedo diffusely reflecting walls [11,12], while the solar concentration produced by specular reflective materials is of an order of magnitude greater, as demonstrated in this paper and by the empirical evidence from relevant case studies listed in Table 1.

Herein, we argue that outdoor thermal comfort models should be enhanced to represent the directional components of the reflection of solar radiation. Furthermore, development control plans and building codes should include a threshold on solar concentration by buildings in order to avert a radiatively induced urban heat island. In fact, a review of more than 220 projects reports a peak ambient temperature reduction by approximately 2 °C when the albedo of an urban area is increased by 0.3 [9]. This also means that decreasing the amount of solar radiation that escapes the urban canopy layer due to downward reflection increases the ambient temperature. The ambient temperature increase caused by specular reflective (glazed) facades is to be determined, but the canyon albedo with specular reflectors and glazed facades is known [63]. If the façade is fully glazed, with a high window to wall ratio, the canyon albedo is lower than 0.05 with high solar elevations [63], while it is more than 0.15 with wall albedos of 0.50 (as also documented experimentally [64]). Additionally, values lower than 0.10 for the canyon albedo are computed when walls are covered by purely specular reflectors [65]. Therefore, fully glazed facades may decrease the urban albedo by approximately 0.10–0.15, thus leading to ambient temperature increases of the order of magnitude of 0.6–0.7 °C, based on the mitigation reported in the literature with increases in urban albedo [9].

5. Conclusions

We analyzed the impact of building geometries and reflection behavior of finishing materials (i.e., diffuse or specular) on the irradiance values measured at street level. The three selected representative geometries (curved convex, vertical flat, and 10% tilted flat) coupled with two different façade materials suggested avoiding caustic curve formation and that the effect of highly reflective surfaces is perceived differently in accordance with the distance from the building.

The measurements taken were an example of the two extreme possible behaviors for approximately Lambertian and specular reflective materials. In a real scenario, the glazing facade material has a behavior that is not perfectly matching both of the boundaries, but rather is in the middle. For a high angle of solar incident radiation, its behavior became almost similar to that of the specular one.

For all these reasons, it is recommended that designers perform a detailed study of the consequences of the materials used for the building envelope during the design phase in accordance with the building context to avoid severe comfort and visual issues in the surroundings of the buildings. In the case of severe impairment, any kind of

post-construction mitigation strategy could be impossible, inadequately expensive, or incompatible with the building architecture. All the façades can be critical, and the coupled effect of the wrong geometry and material choices can magnify glare and solar concentration problems. For these reasons, all the surrounding areas particularly sensitive to the reflected light must be carefully identified to understand the impact that reflected sunlight can have on safety and comfort issues.

Among the alternatives, a speditive evaluation (both in the preliminary and construction phase) can be performed by using a parametric script to evaluate any surface under a general orientation only by changing the cone amplitude, as described in Section 2.3.2. This approach can enhance the design of complex envelopes, providing the possibility to evaluate the amount of reflected radiation and, indirectly, to know how much energy is passing through the surface in case of a glazed façade.

The proposed method helps to understand which glazed units can be problematic and for how many hours, enhancing the design by developing shading strategies.

Future developments of the test and procedure presented can facilitate the analysis of other geometries and materials and be applied to shading strategies such as local overhangs, fins, and external shading systems that can mitigate or exclude critical sunlight reflections, considering sensitive areas as local constraints.

The relevance of this study concerns two aspects. We evaluated the impact of tall buildings and their geometry, with the quantification of solar concentration by archetypical combinations of façade geometry and materials and the identification of a measurement protocol. This research also sheds light on the need for considering solar concentration in research on urban overheating. With an increasing use of specularly reflective materials in the built environment, urban climate models need to embed this capability beyond what has already been reported in studies supporting the performance analysis of retro-reflective materials.

Author Contributions: Conceptualization, A.S., A.G.M., A.Z., R.P. and T.P. (Tiziana Poli); methodology, A.S., A.G.M., A.Z., R.P. and T.P. (Tiziana Poli); validation, A.S., A.G.M., A.Z. and R.P.; formal analysis, A.S., A.G.M., A.Z., R.P. and T.P. (Tommaso Pagnacco); investigation, A.S., A.G.M., A.Z., R.P., T.P. (Tommaso Pagnacco) and T.P. (Tiziana Poli); data curation, A.S., A.G.M., A.Z. and R.P.; writing—original draft preparation, A.S., A.G.M., A.Z. and R.P.; writing—review and editing, A.S., A.G.M., A.Z., R.P., T.P. (Tommaso Pagnacco) and T.P. (Tiziana Poli); visualization, A.S., A.G.M., A.Z. and T.P. (Tommaso Pagnacco); supervision, T.P. (Tiziana Poli); project administration, T.P. (Tiziana Poli); funding acquisition, T.P. (Tiziana Poli). All authors have read and agreed to the published version of the manuscript.

Funding: This work was funded in part by Politecnico di Milano with the program “Fondi ricerca di base”, in part by the Italian Ministry for Economic Development with the projects “Valutazione delle prestazioni di cool materials esposti all’ambiente urbano” and “Sviluppo di materiali e tecnologie per la riduzione degli effetti della radiazione solare”, and in part by the Italian Ministry of Education, University and Research with the project “PRINSense”.

Institutional Review Board Statement: Not applicable.

Informed Consent Statement: Not applicable.

Data Availability Statement: All the data collected are reported in Appendices A–F.

Acknowledgments: This work has been made possible thanks to the measurement instruments given by Elisabetta Rosina and by SEED Lab and the partnership of PA&CO Architecture for the mock-up design and production. The authors thank Osservatorio Meteo Milano Duomo for the validation of weather data and solar radiation data. A special thanks to Michele Alghisi, who helped us during all the measurement phases, and to Vittoria Sykopetrites for reviewing the manuscript.

Conflicts of Interest: The authors declare no conflict of interest.

Appendix A. Flat Diffusive Façade



Figure A1. Flat diffusive façade—Experimental setup and measurement points position (Figure 2).

Table A1. Irradiance and Unit of sun per each measurement point over the sample plane. All the measurements have been performed on the 19 of September with the exception of the underlined number that refers to the 21 September.

Start Time	End Time	MIN N.d.	MAX N.d.	A	B	C	D	E	F	G	H	I	L	M	N	O	P
[hh:mm]	[hh:mm]	[W/m ²]	[W/m ²]	The Upper Value Refers to the Measure in Each Point [W/m ²] While the Lower Is the Ratio [-] with the Undisturbed Measure (Unit of Sun)													
9:00	9:15	254	294	267	323	310	292	339	337	333	328	333	316	321	338	346	336
				1.27	1.21	1.11	1.27	1.24	1.21	1.16	1.17	1.09	1.09	1.13	1.13	1.09	
10:00	10:16	420	458	430	521	495	458	504	517	506	490	495	478	483	505	509	492
				1.24	1.16	1.06	1.16	1.18	1.15	1.10	1.10	1.06	1.06	1.10	1.10	1.10	1.05
11:00	11:17	549	578	556	673	628	585	627	657	640	614	620	600	597	625	625	602
				1.23	1.14	1.06	1.13	1.18	1.14	1.09	1.10	1.06	1.05	1.09	1.09	1.09	1.05
<u>12:03</u>	<u>12:20</u>	<u>654</u>	<u>676</u>	<u>647</u>	<u>799</u>	<u>753</u>	<u>695</u>	<u>717</u>	<u>748</u>	<u>743</u>	<u>723</u>	<u>732</u>	<u>710</u>	<u>650</u>	<u>711</u>	<u>739</u>	<u>703</u>
				<u>1.22</u>	<u>1.15</u>	<u>1.06</u>	<u>1.09</u>	<u>1.13</u>	<u>1.12</u>	<u>1.09</u>	<u>1.10</u>	<u>1.06</u>	<u>0.97</u>	<u>1.06</u>	<u>1.06</u>	<u>1.10</u>	<u>1.04</u>
13:02	13:18	546	734	732	895	832	761	773	830	798	754	760	747	749	784	790	755
				1.64	1.45	1.27	1.18	1.22	1.13	1.03	1.04	1.02	1.02	1.07	1.08	1.04	
14:00	14:16	690	712	695	852	789	727	713	766	732	706	720	713	721	754	761	727
				1.20	1.11	1.03	1.01	1.09	1.05	1.01	1.04	1.03	1.04	1.09	1.10	1.05	
15:00	15:15	631	656	648	782	720	680	655	696	671	649	667	656	655	684	691	672
				1.19	1.10	1.04	1.01	1.07	1.04	1.01	1.04	1.03	1.03	1.08	1.09	1.06	
16:00	16:18	510	570	550	656	591	575	527	550	525	512	530	520	535	553	560	540
				1.15	1.05	1.03	0.97	1.02	0.99	0.97	1.01	1.00	1.03	1.07	1.09	1.05	
17:00	17:17	347	398	374	461	421	420	364	376	356	344	360	361	365	374	378	361
				1.16	1.07	1.08	0.94	0.98	0.94	0.91	0.96	0.98	1.00	1.05	1.07	1.03	

Appendix B. Flat Reflective Façade



Figure A2. Flat reflective façade—Experimental setup and measurement points position (Figure 2).

Table A2. Irradiance and Unit of sun per each measurement point over the sample plane. All the measurements have been performed on the 25 September.

Start Time	End Time	MIN N.d.	MAX N.d.	A	B	C	D	E	F	G	H	I	L	M	N	O	P
[hh:mm]	[hh:mm]	[W/m ²]	[W/m ²]	The Upper Value Refers to the Measure in Each Point [W/m ²] While the Lower Is the Ratio [-] with the Undisturbed Measure (Unit of Sun)													
9:00	9:11	256	279	248	255	263	467	304	282	285	294	297	403	281	281	280	278
				1.00	1.02	1.80	1.15	1.06	1.06	1.08	1.09	1.47	1.01	1.00	0.99	0.98	
10:00	10:10	416	439	406	422	754	431	467	445	444	450	458	439	870	441	438	437
				1.02	1.81	1.03	1.11	1.05	1.04	1.05	1.06	1.02	2.00	1.01	0.99	0.98	
11:00	11:11	550	563	540	905	987	557	590	575	575	580	592	572	1099	1075	564	557
				1.65	1.79	1.01	1.06	1.04	1.03	1.03	1.05	1.02	1.95	1.91	0.99	0.97	
12:05	12:16	653	662	661	1179	1201	657	680	677	676	673	688	675	663	1294	1190	662
				1.81	1.84	1.01	1.04	1.03	1.02	1.02	1.04	1.02	1.00	1.96	1.80	1.00	
13:06	13:17	676	686	693	1321	705	698	694	708	711	691	697	686	685	704	1327	1374
				1.92	1.03	1.02	1.01	1.03	1.04	1.01	1.02	1.01	1.01	1.04	1.94	2.01	
14:01	14:1	660	669	672	1290	680	682	667	1242	1259	665	688	677	671	675	684	667
				1.92	1.02	1.02	1.00	1.86	1.90	1.01	1.04	1.03	1.02	1.02	1.03	1.01	
15:18	15:24	558	565	569	602	576	585	558	1075	565	1309	582	578	573	573	571	563
				1.05	1.02	1.04	1.00	1.93	1.01	2.33	1.03	1.02	1.02	1.02	1.02	1.01	
16:14	16:23	428	449	462	481	468	486	455	782	428	635	453	445	442	440	440	435
				1.06	1.04	1.08	1.02	1.75	0.97	1.45	1.03	1.02	1.02	1.03	1.03	1.02	
16:57	17:08	308	334	334	347	339	359	525	314	296	297	462	314	313	310	311	308
				1.03	1.01	1.09	1.60	0.97	0.92	0.93	1.46	1.00	1.00	1.01	1.02	1.02	

Appendix C. Flat 10% Tilted Diffusive Façade



Figure A3. Flat 10% tilted diffusive façade—Experimental setup and measurement points position (Figure 2).

Table A3. Irradiance and Unit of sun per each measurement point over the sample plane. All the measurements have been performed on the 21 September.

Start Time	End Time	MIN N.d.	MAX N.d.	A	B	C	D	E	F	G	H	I	L	M	N	O	P
[hh:mm]	[hh:mm]	[W/m ²]	[W/m ²]	The Upper Value Refers to the Measure in Each Point [W/m ²] While the Lower Is the Ratio [-] with the Undisturbed Measure (Unit of Sun)													
9:03	9:19	257	302	268	329	311	289	342	340	343	333	329	316	311	328	329	318
				1.28	1.20	1.10	1.29	1.26	1.25	1.20	1.16	1.10	1.07	1.12	1.11	1.05	
10:00	10:21	426	474	430	534	500	457	500	516	518	499	498	485	482	509	513	490
				1.28	1.17	1.07	1.15	1.18	1.18	1.13	1.12	1.08	1.06	1.11	1.11	1.05	
11:18	11:33	590	605	595	744	687	614	652	685	674	639	656	638	642	671	678	636
				1.27	1.16	1.04	1.10	1.15	1.13	1.07	1.10	1.06	1.07	1.12	1.12	1.05	
12:23	12:39	685	702	692	848	798	715	725	795	775	735	745	727	728	771	774	733
				1.24	1.16	1.04	1.05	1.14	1.11	1.06	1.07	1.04	1.04	1.10	1.10	1.04	
13:00	-	-	-	-	-	-	-	-	-	-	-	-	-	-	-	-	-
				-	-	-	-	-	-	-	-	-	-	-	-	-	-
14:06	14:51	554	690	686	850	790	735	713	775	735	702	710	699	694	726	730	690
				1.23	1.15	1.07	1.04	1.13	1.33	1.24	1.20	1.16	1.12	1.15	1.14	1.08	
15:01	15:16	620	630	632	686	720	673	652	702	673	641	648	642	643	675	683	651
				1.09	1.15	1.07	1.04	1.12	1.07	1.02	1.03	1.02	1.03	1.08	1.10	1.05	
16:01	16:32	425	498	516	646	587	566	524	557	530	443	456	453	468	487	498	463
				1.30	1.19	1.16	1.09	1.17	1.14	1.04	1.06	1.05	1.07	1.10	1.14	1.07	
17:00	17:13	333	356	340	426	392	395	343	369	351	339	348	348	349	358	363	349
				1.16	1.10	1.11	0.97	1.05	1.00	0.97	1.01	1.01	1.02	1.05	1.07	1.04	

Appendix D. Flat 10% Tilted Reflective Façade

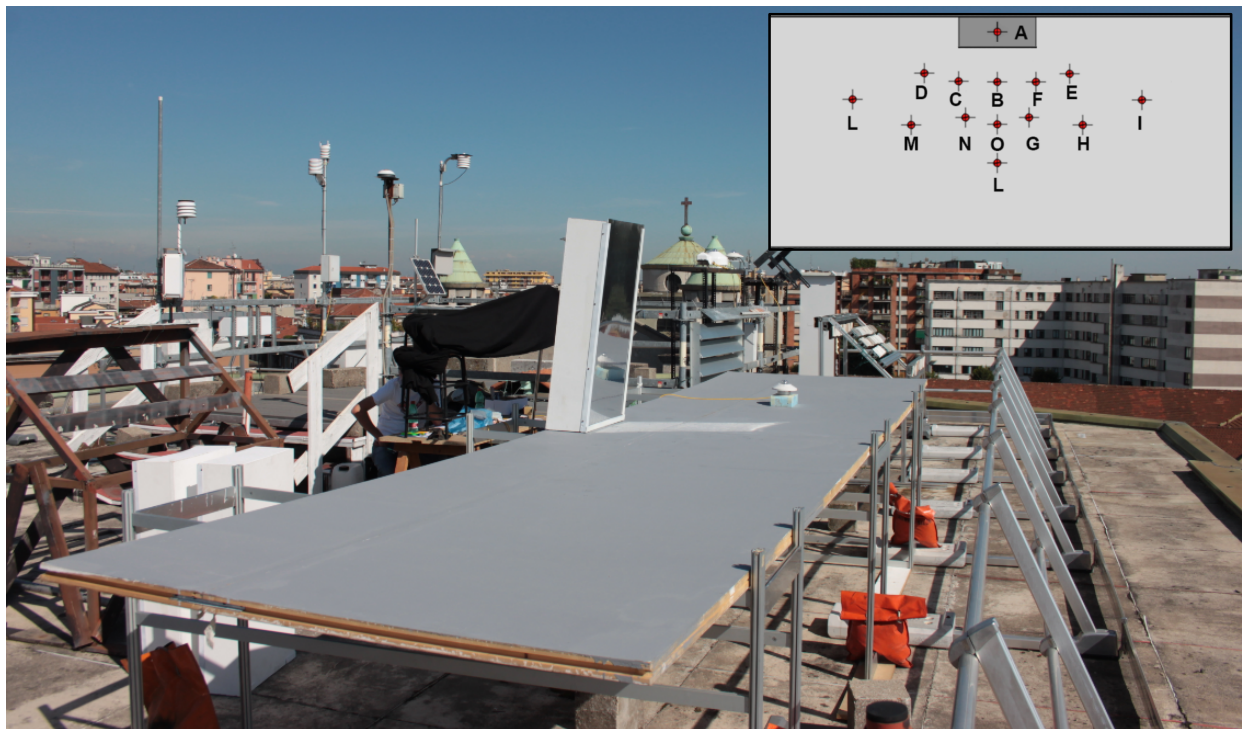


Figure A4. Flat 10% tilted diffusive façade—Experimental setup and measurement points position (Figure 2).

Table A4. Irradiance and Unit of sun per each measurement point over the sample plane. All the measurements have been performed on the 25 September.

Start Time	End Time	MIN N.d.	MAX N.d.	A	B	C	D	E	F	G	H	I	L	M	N	O	P
[hh:mm]	[hh:mm]	[W/m ²]	[W/m ²]	The Upper Value Refers to the Measure in Each Point [W/m ²] While the Lower Is the Ratio [-] with the Undisturbed Measure (Unit of Sun)													
9:17	9:28	302	328	292	312	509	487	363	337	337	344	346	437	331	332	331	329
				1.05	1.68	1.59	1.18	1.08	1.07	1.08	1.08	1.36	1.02	1.01	1.00	0.98	
10:20	10:31	469	490	455	494	846	488	526	503	504	508	518	500	906	512	498	492
				1.06	1.80	1.04	1.11	1.05	1.05	1.06	1.08	1.03	1.86	1.04	1.01	0.99	
11:20	11:31	588	603	581	1155	1113	596	628	616	614	615	627	613	1002	1146	616	605
				1.97	1.89	1.01	1.06	1.05	1.04	1.03	1.05	1.02	1.67	1.90	1.02	0.99	
12:20	12:31	663	675	654	1292	1337	669	680	696	699	687	697	685	677	1313	1288	680
				1.95	2.02	1.00	1.02	1.04	1.05	1.03	1.05	1.03	1.00	1.95	1.91	1.01	
13:21	13:32	642	685	685	1229	696	682	686	722	1299	686	702	695	688	708	1314	694
				1.79	1.02	1.03	1.06	1.08	1.95	1.01	1.03	1.01	1.03	1.10	1.93	1.02	
14:20	14:31	650	657	656	1219	675	675	658	1249	1232	663	676	667	662	669	679	659
				1.85	1.03	1.03	1.00	1.91	1.89	1.01	1.04	1.02	1.01	1.03	1.04	1.01	
15:27	15:35	540	549	546	976	563	579	551	1159	515	1063	560	554	552	553	558	547
				1.77	1.03	1.06	1.01	2.12	0.95	1.95	1.03	1.02	1.02	1.02	1.03	1.02	
16:27	16:38	390	411	420	435	421	443	414	709	388	394	411	406	401	399	401	398
				1.05	1.02	1.08	1.02	1.75	0.96	0.99	1.04	1.04	1.03	1.02	1.04	1.03	
17:20	17:31	248	270	270	288	280	304	456	263	244	244	604	262	263	259	261	257
				1.05	1.04	1.14	1.74	1.01	0.95	0.95	2.39	1.05	1.05	1.04	1.05	1.05	

Appendix E. Concave Diffusive Façade



Figure A5. Concave diffusive façade—Experimental setup and measurement points position (Figure 2).

Table A5. Irradiance and Unit of sun per each measurement point over the sample plane. All the measurements have been performed on the 19 of September with the exception of the underlined number that refers to the 21 September.

Start Time	End Time	MIN N.d.	MAX N.d.	A	B	B_2	C	D	E	F	G	H	I	L	M	N	O	P
[hh:mm]	[hh:mm]	[W/m ²]	[W/m ²]	The Upper Value Refers to the Measure in Each Point [W/m ²] While the Lower Is the Ratio [-] with the Undisturbed Measure (Unit of Sun)														
9:28	9:47	335	384	351	413	-	402	373	417	416	412	405	410	395	397	417	419	407
				1.23	-	1.18	1.09	1.19	1.18	1.15	1.12	1.12	1.06	1.06	1.10	1.10	1.10	1.06
10:26	10:49	494	530	511	604	625	574	530	573	586	575	559	564	543	545	571	573	550
				1.23	1.26	1.16	1.06	1.14	1.15	1.13	1.09	1.09	1.04	1.04	1.09	1.09	1.09	1.04
11:41	11:57	623	645	618	744	798	725	664	693	731	715	686	693	658	665	694	708	677
				1.20	1.28	1.16	1.06	1.10	1.16	1.13	1.08	1.09	1.03	1.04	1.08	1.10	1.05	
12:45	13:01	694	708	713	815	841	792	729	754	801	779	734	751	726	720	762	760	692
				1.17	1.21	1.14	1.05	1.09	1.15	1.12	1.05	1.07	1.03	1.02	1.08	1.07	0.98	
13:30	13:44	716	720	733	865	898	809	741	740	795	773	740	751	739	740	775	780	746
				1.20	1.25	1.12	1.03	1.03	1.11	1.08	1.03	1.05	1.03	1.03	1.08	1.09	1.04	
14:31	14:46	663	668	669	800	831	746	701	682	734	711	682	690	683	690	720	730	701
				1.20	1.24	1.12	1.05	1.02	1.10	1.07	1.03	1.04	1.03	1.04	1.09	1.10	1.06	
16:28	16:44	441	476	480	572	576	506	498	447	472	447	432	447	449	456	470	476	458
				1.18	1.20	1.06	1.05	0.95	1.01	0.97	0.95	0.99	1.00	1.02	1.06	1.08	1.04	
17:30	17:44	262	296	295	341	345	304	314	258	274	256	251	264	273	275	279	282	270
				1.13	1.15	1.03	1.07	0.90	0.97	0.92	0.91	0.97	1.01	1.03	1.05	1.08	1.04	

Appendix F. Concave Reflective Façade

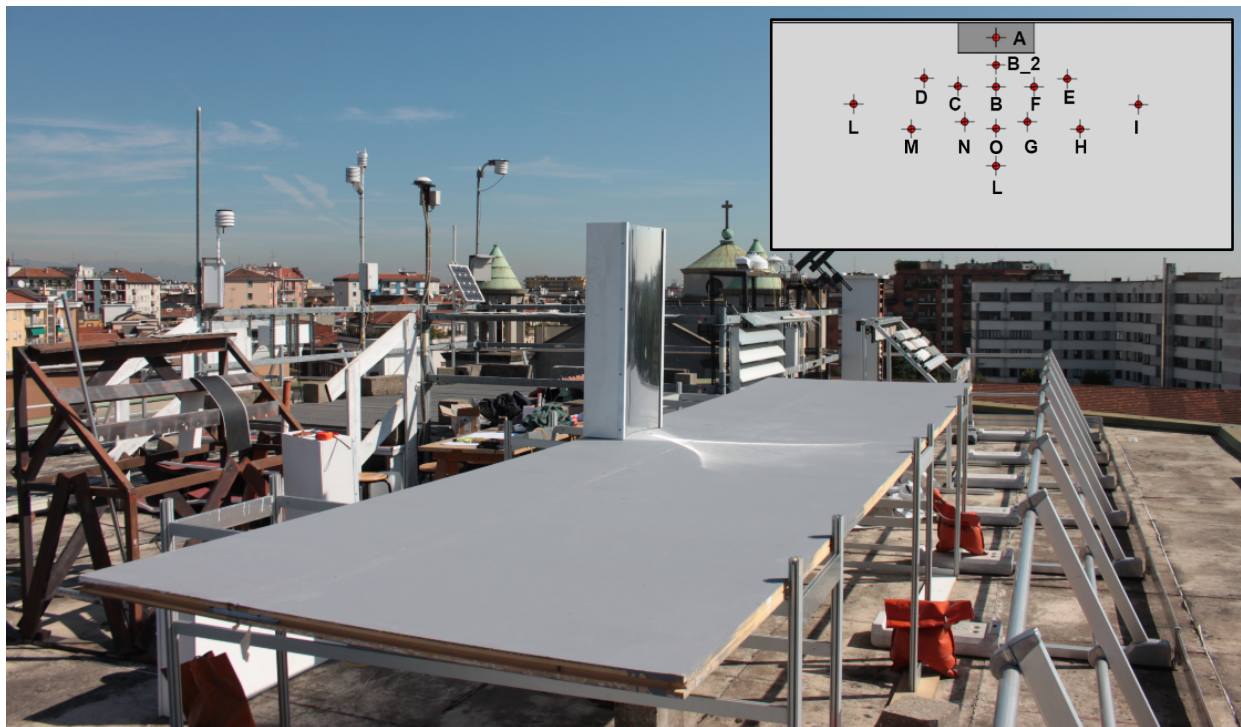


Figure A6. Concave reflective façade—Experimental setup and measurement points position (Figure 2).

Table A6. Irradiance and Unit of sun per each measurement point over the sample plane. All the measurements have been performed on the 25 September.

Start Time	End Time	MIN N.d.	MAX N.d.	A	B	B_2	C	D	E	F	G	H	I	L	M	N	O	P
[hh:mm]	[hh:mm]	[W/m ²]	[W/m ²]	The Upper Value Refers to the Measure in Each Point [W/m ²] While the Lower Is the Ratio [-] with the Undisturbed Measure (Unit of Sun)														
9:35	9:53	350	397	341	370	375	394	450	419	396	395	404	409	422	464	389	386	384
				1.01	1.0207	1.07	1.21	1.12	1.05	1.05	1.07	1.07	1.1	1.2	1	0.99	0.99	
10:42	10:55	512	539	517	526	533	1402	865	562	545	544	549	560	608	668	553	536	529
				1.02	1.03	2.71	1.67	1.08	1.05	1.04	1.05	1.07	1.15	1.26	1.04	1.00	0.99	
11:41	11:56	620	634	631	651	667	690	631	657	650	649	648	663	649	853	1022	647	637
				1.04	1.07	1.10	1.00	1.04	1.03	1.03	1.03	1.05	1.03	1.35	1.62	1.02	1.00	
12:42	12:56	678	689	689	1286	1521	696	680	694	701	702	696	713	701	687	718	1103	812
				1.90	2.24	1.03	1.00	1.02	0.00	1.03	1.03	1.01	1.03	1.02	1.00	1.05	1.62	
13:40	13:48	674	682	692	1055	1823	695	689	686	702	1492	686	704	694	687	693	752	1089
				1.55	2.68	1.02	1.01	1.01	1.03	2.18	1.00	1.03	1.02	1.01	1.02	1.11	1.61	
15:07	15:17	573	601	611	620	627	606	617	602	1095	607	681	623	590	-	-	592	-
				1.03	1.05	1.01	1.04	1.01	1.85	1.04	1.17	1.07	1.02	-	-	1.04	-	
15:37	15:44	518	533	547	554	557	540	557	719	1237	522	653	571	534	531	531	533	527
				1.05	1.06	1.03	1.06	1.37	2.37	1.00	1.25	1.09	1.03	1.02	1.02	1.03	1.02	
16:45	16:55	346	372	379	383	384	376	396	380	363	340	569	433	360	358	354	355	351
				1.04	1.05	1.03	1.09	1.04	1.00	0.95	1.60	1.23	1.02	1.03	1.02	1.03	1.02	
17:37	17:47	197	228	237	237	231	251	238	203	192	196	225	214	213	208	210	208	
				1.04	1.04	1.03	1.14	1.10	0.94	0.91	0.94	1.09	1.05	1.05	1.04	1.07	1.06	

References

1. Santamouris, M.; Vasilakopoulou, K. Present and Future Energy Consumption of Buildings: Challenges and Opportunities towards Decarbonisation. *e-Prime* **2021**, *1*, 100002. [CrossRef]
2. Zhang, J.; Mohegh, A.; Li, Y.; Levinson, R.; Ban-Weiss, G. Systematic Comparison of the Influence of Cool Wall versus Cool Roof Adoption on Urban Climate in the Los Angeles Basin. *Environ. Sci. Technol.* **2018**, *52*, 11188–11197. [CrossRef] [PubMed]
3. Zhang, Y.; Long, E.; Li, Y.; Li, P. Solar radiation reflective coating material on building envelopes: Heat transfer analysis and cooling energy saving. *Energy Explor. Exploit.* **2017**, *35*, 748–766. [CrossRef]
4. Akbari, H.; Pomerantz, M.; Taha, H. Cool surfaces and shade trees to reduce energy use and improve air quality in urban areas. *Sol. Energy* **2001**, *70*, 295–310. [CrossRef]
5. Akbari, H. Measured energy savings from the application of reflective roofs in two small non-residential buildings. *Energy* **2003**, *28*, 953–967. [CrossRef]
6. Akbari, H.; Konopacki, S. Calculating energy-saving potentials of heat-island reduction strategies. *Energy Policy* **2005**, *33*, 721–756. [CrossRef]
7. Synnefa, A.; Santamouris, M.; Akbari, H. Estimating the effect of using cool coatings on energy loads and thermal comfort in residential buildings in various climatic conditions. *Energy Build.* **2007**, *39*, 1167–1174. [CrossRef]
8. Santamouris, M. Cooling the cities—A review of reflective and green roof mitigation technologies to fight heat island and improve comfort in urban environments. *Sol. Energy* **2014**, *103*, 682–703. [CrossRef]
9. Santamouris, M.; Ding, L.; Fiorito, F.; Oldfield, P.; Osmond, P.; Paolini, R.; Prasad, D.; Synnefa, A. Passive and active cooling for the outdoor built environment—Analysis and assessment of the cooling potential of mitigation technologies using performance data from 220 large scale projects. *Sol. Energy* **2017**, *154*, 14–33. [CrossRef]
10. Zinzi, M. Exploring the potentialities of cool facades to improve the thermal response of Mediterranean residential buildings. *Sol. Energy* **2016**, *135*, 386–397. [CrossRef]
11. Lee, H.; Mayer, H. Thermal comfort of pedestrians in an urban street canyon is affected by increasing albedo of building walls. *Int. J. Biometeorol.* **2018**, *62*, 1199–1209. [CrossRef] [PubMed]
12. Nazarian, N.; Dumas, N.; Kleissl, J.; Norford, L. Effectiveness of cool walls on cooling load and urban temperature in a tropical climate. *Energy Build.* **2019**, *187*, 144–162. [CrossRef]
13. Rossi, F.; Pisello, A.L.; Nicolini, A.; Filipponi, M.; Palombo, M. Analysis of retro-reflective surfaces for urban heat island mitigation: A new analytical model. *Appl. Energy* **2014**, *114*, 621–631. [CrossRef]
14. Rossi, F.; Morini, E.; Castellani, B.; Nicolini, A.; Bonamente, E.; Anderini, E.; Cotana, F. Beneficial effects of retroreflective materials in urban canyons: Results from seasonal monitoring campaign. *J. Phys. Conf. Ser.* **2015**, *655*, 12012. [CrossRef]
15. Yuan, J.; Farnham, C.; Emura, K. Development of a retro-reflective material as building coating and evaluation on albedo of urban canyons and building heat loads. *Energy Build.* **2015**, *103*, 107–117. [CrossRef]
16. Levinson, R.; Chen, S.; Slack, J.; Goudey, H.; Harima, T.; Berdahl, P. Design, characterization, and fabrication of solar-retroreflective cool-wall materials. *Sol. Energy Mater. Sol. Cells* **2020**, *206*, 110117. [CrossRef]
17. Yang, S.-H.; Matzarakis, A. Study on human thermal comfort for architecture—The Example of Shanghai, China. In Proceedings of the ICUC9—9th International Conference on Urban Climate, Toulouse, France, 20–24 July 2015.
18. Matzarakis, A.; Fröhlich, D.; Gangwisch, M.; Ketterer, C.; Peer, A.; Freiburg, A.; Freiburg, D. Developments and applications of thermal indices in urban structures by RayMan and SkyHelios model. In Proceedings of the ICUC9—9th International Conference on Urban Climate, Toulouse, France, 20–24 July 2015.
19. Schiler, M.; Valmont, E. Microclimatic impact: Glare around the Walt Disney Concert Hall. In Proceedings of the Solar World Congress 2005 Joint American Solar Energy Society/International Solar Energy Conference, Orlando, 6–12 August 2005; p. 511.
20. Furler, R.A. Angular Dependence of Optical Properties of Homogeneous Glasses. *ASHRAE Trans.* **1991**, *98*, 1.
21. CityA.M. Dazzling Shard Has Inadvertent Effect of Blinding Train Drivers. 2012. Available online: <https://www.cityam.com/dazzling-shard-has-inadvertent-effect-blinding-train-drivers/> (accessed on 20 January 2022).
22. Rose, T.; Wollert, A. The dark side of photovoltaic—3D simulation of glare assessing risk and discomfort. *Environ. Impact Assess. Rev.* **2015**, *52*, 24–30. [CrossRef]
23. Ho, C.K.; Ghanbari, C.M.; Diver, R.B. Methodology To Assess Potential Glint and Glare Hazards From Concentrating Solar Power Plants: Analytical Models and Experimental Validation. *J. Sol. Energy Eng.* **2011**, *133*, 3102. [CrossRef]
24. Las Vegas Review Journal. Vdara Visitor: ‘Death Ray’ Scorched Hair. 2010. Available online: <https://www.reviewjournal.com/news/vdara-visitor-death-ray-scorched-hair/> (accessed on 20 January 2022).
25. Pexels. Available online: <https://www.pexels.com/> (accessed on 16 March 2022).
26. Campbell-Dollaghan, K. A Brief History of Buildings That Melt Things. Available online: <https://gizmodo.com/a-brief-history-of-buildings-that-melt-things-1247657178> (accessed on 20 January 2022).
27. Danks, R.; Good, J. Urban Scale Simulations of Solar Reflections in the Built Environment: Methodology & Validation. In Proceedings of the Symposium on Simulation for Architecture & Urban Design 2016, London, UK, 16–18 May 2016; pp. 19–26.
28. Danks, R.; Good, J.; Sinclair, R. Assessing reflected sunlight from building facades: A literature review and proposed criteria. *Build. Environ.* **2016**, *103*, 193–202. [CrossRef]

29. Development Control Plan. Section 3 General Provisions, Sydney, AU. 2012. Available online: https://www.cityofsydney.nsw.gov.au/-/media/corporate/files/2020-07-migrated/files_s-1/section3-dcp2012-170619.pdf?download=true (accessed on 16 March 2022).
30. Buildings Department. *Guidelines on Design and Construction Requirements for Energy Efficiency of Residential Buildings*; Buildings Department: Hong Kong, 2014.
31. Dwyer, C. *Planning Advice Note Solar Glare: Guidelines and Best Practice for Assessing Solar Glare in the City of London*; The City of London Corporation: London, UK, 2017.
32. Suk, J.Y.; Schiler, M.; Kensek, K. Is Exterior Glare Problematic? Investigation on Visual Discomfort Caused by Reflected Sunlight on Specular Building Facades. In Proceedings of the PLEA 2016 Conference on Passive and Low energy Architecture. Cities, buildings, People: Towards Regenerative Environments, Los Angeles, CA, USA, 11–13 July 2016.
33. Shih, N.J.; Huang, Y.S. A study of reflection glare in Taipei. *Build. Res. Inf.* **2001**, *29*, 30–39. [[CrossRef](#)]
34. Danks, R.; Good, J. Urban Solar Reflection Identification, Simulation, Analysis and Mitigation: Learning From Case Studies. In Proceedings of the eSim 2016 Building Performance Simulation Conference eSim 2016, Hamilton, ON, Canada, 3–6 May 2016; pp. 309–318.
35. Brzezicki, M. The Influence of Reflected Solar Glare Caused by the Glass Cladding of a Building: Application of Caustic Curve Analysis. *Comput. Civ. Infrastruct. Eng.* **2012**, *27*, 347–357. [[CrossRef](#)]
36. Yang, X.; Grobe, L.; Stephen, W. Simulation of Reflected Daylight From Building Envelopes. In Proceedings of the 13th Conference of International Building Performance Simulation Association, Chambéry, France, 26–28 August 2013; pp. 3673–3680.
37. Ou, Y. Quantitative study of reflection of sunlight by a glass curtain wall resulting in a visual masking effect. *Appl. Opt.* **2014**, *53*, 6893. [[CrossRef](#)] [[PubMed](#)]
38. Shih, N.J.; Huang, Y.-S. An analysis and simulation of curtain wall reflection glare. *Build. Environ.* **1999**, *36*, 619–626. [[CrossRef](#)]
39. Vollmer, M.; Möllmann, K.P. Caustic effects due to sunlight reflections from skyscrapers: Simulations and experiments. *Eur. J. Phys.* **2012**, *33*, 1429–1455. [[CrossRef](#)]
40. POV-Ray. Available online: <http://www.povray.org/> (accessed on 16 March 2022).
41. OpticStudio. Available online: <https://www.zemax.com/pages/opticstudio> (accessed on 16 March 2022).
42. Ishak, N.M.; Hien, W.N.; Jenatabadi, H.S.; Mustafa, N.A.; Zawawi, E.M.A. Effect of reflective building façade on pedestrian visual comfort. *IOP Conf. Ser. Earth Environ. Sci.* **2019**, *385*, 12059. [[CrossRef](#)]
43. Achسانی, R.A.; Wonorahardjo, S. Studies on Visual Environment Phenomena of Urban Areas: A Systematic Review. *IOP Conf. Ser. Earth Environ. Sci.* **2020**, *532*, 12016. [[CrossRef](#)]
44. Wong, J.S.J. A comprehensive ray tracing study on the impact of solar reflections from glass curtain walls. *Environ. Monit. Assess.* **2016**, *188*, 16. [[CrossRef](#)]
45. Danks, R.; Good, J.; Sinclair, R. Avoiding The Dreaded Death Ray: Controlling Facade Reflections through Purposeful Design. In Proceedings of the Façade Tectonics World Congress, Los Angeles, CA, USA, 2016; Volume 2, ISBN 978-1-882352-43-2. Available online: https://www.researchgate.net/publication/309136628_Avoiding_The_Dreaded_Death_Ray_Controlling_Facade_Reflections_Through_Purposeful_Design (accessed on 16 March 2022).
46. McNeel Rhinoceros. Available online: <https://www.rhino3d.com/> (accessed on 16 March 2022).
47. Grasshopper for Rhinoceros. Available online: <https://www.grasshopper3d.com/> (accessed on 16 March 2022).
48. Barr, J. Skyscraper Height. *J. Real Estate Financ. Econ.* **2012**, *45*, 723–753. [[CrossRef](#)]
49. UNI—Ente Italiano di Normazione. *UNI EN 14500—Benessere Termico E Visivo, Metodi Di Prova E Di Calcolo*; UNI—Ente Italiano di Normazione: Milano, Italy, 2021.
50. ASTM International (ASTM). *ASTM E903—Standard Test Method for Solar Absorptance, Reflectance, and Transmittance of Materials Using Integrating Spheres*; ASTM International: West Conshohocken, PA, USA, 2020; p. 17.
51. Masson, V.; Grimmond, C.S.B.; Oke, T.R. Evaluation of the Town Energy Balance (TEB) Scheme with Direct Measurements from Dry Districts in Two Cities. *J. Appl. Meteorol.* **2002**, *41*, 1011–1026. [[CrossRef](#)]
52. Lemonsu, A.; Grimmond, C.S.B.; Masson, V. Modeling the Surface Energy Balance of the Core of an Old Mediterranean City: Marseille. *J. Appl. Meteorol.* **2004**, *43*, 312–327. [[CrossRef](#)]
53. Ban-Weiss, G.A.; Woods, J.; Levinson, R. Using remote sensing to quantify albedo of roofs in seven California cities, Part 1: Methods. *Sol. Energy* **2015**, *115*, 777–790. [[CrossRef](#)]
54. LBNL WINDOW Version 7.7.16. Available online: <https://windows.lbl.gov/software/window> (accessed on 16 March 2022).
55. González, J.; Fiorito, F. Daylight Design of Office Buildings: Optimisation of External Solar Shadings by Using Combined Simulation Methods. *Buildings* **2015**, *5*, 560–580. [[CrossRef](#)]
56. Duffie, J.; Beckman, W. *Solar Engineering of Thermal Processes*, 4th ed.; John Wiley & Sons: Hoboken, NJ, USA, 2013; ISBN 9780470873663.
57. Takebayashi, H. High-reflectance technology on building façades: Installation guidelines for pedestrian comfort. *Sustainability* **2016**, *8*, 785. [[CrossRef](#)]
58. Shanks, K.; Ferrer-Rodríguez, J.P.; Fernández, E.F.; Almonacid, F.; Pérez-Higueras, P.; Senthilarasu, S.; Mallick, T. A >3000 suns high concentrator photovoltaic design based on multiple Fresnel lens primaries focusing to one central solar cell. *Sol. Energy* **2018**, *169*, 457–467. [[CrossRef](#)]

59. Gordon, J.M. A 100-sun linear photovoltaic solar concentrator design from inexpensive commercial components. *Sol. Energy* **1996**, *57*, 301–305. [[CrossRef](#)]
60. Paolini, R.; Terraneo, G.; Ferrari, C.; Sleiman, M.; Muscio, A.; Metrangolo, P.; Poli, T.; Destailats, H.; Zinzi, M.; Levinson, R. Effects of soiling and weathering on the albedo of building envelope materials: Lessons learned from natural exposure in two European cities and tuning of a laboratory simulation practice. *Sol. Energy Mater. Sol. Cells* **2020**, *205*, 110264. [[CrossRef](#)]
61. Wang, J.; Liu, S.; Meng, X.; Gao, W.; Yuan, J. Application of retro-reflective materials in urban buildings: A comprehensive review. *Energy Build.* **2021**, *247*, 111137. [[CrossRef](#)]
62. Yuan, J.; Emura, K.; Farnham, C. Evaluation of retro-reflective properties and upward to downward reflection ratio of glass bead retro-reflective material using a numerical model. *Urban Clim.* **2021**, *36*, 100774. [[CrossRef](#)]
63. Tsangrassoulis, A.; Santamouris, M. Numerical estimation of street canyon albedo consisting of vertical coated glazed facades. *Energy Build.* **2003**, *35*, 527–531. [[CrossRef](#)]
64. Kotopouleas, A.; Giridharan, R.; Nikolopoulou, M.; Watkins, R.; Yeninarçilar, M. Experimental investigation of the impact of urban fabric on canyon albedo using a 1:10 scaled physical model. *Sol. Energy* **2021**, *230*, 449–461. [[CrossRef](#)]
65. Aida, M.; Gotoh, K. Urban albedo as a function of the urban structure—A two-dimensional numerical simulation—Part II. *Bound. Layer Meteorol.* **1982**, *23*, 415–424. [[CrossRef](#)]